*Astronomy & Astrophysics* manuscript no. output
July 5, 2026


# DUETS II – RG asteroseismic binaries confirmed with spectroscopy

J. S. Thomsen[1⋆], W. E. van Rossem[2,1], A. Miglio[1,3], A. Mazzi[1], V. D'Orazi[4,5], W. Ball[6], M. Tailo[1,3], M. Matteuzzi[1,3], E. Corsaro[7], K. Brogaard[8], M. Marcussen[8], M. N. Lund[8], F. Grundahl[8], E. Knudstrup[8], and D. Slumstrup[9,10]

[1] Department of Physics and Astronomy "Augusto Righi", University of Bologna, via Gobetti 93/2, 40129, Bologna, Italy
[2] Departament d'Astronomia i Astrofísica, Universitat de València, C. Dr. Moliner 50, 46100 Burjassot, Spain
[3] Osservatorio di Astrofisica e Scienza dello Spazio di Bologna, INAF, Via Gobetti 93/3, Bologna, 40129, Italia
[4] Dept. of Physics, University of Rome Tor Vergata, via della Ricerca Scientifica 1, 00133, Rome, Italy
[5] INAF Osservatorio Astronomico di Roma, via Frascati 33, 00078, Monte Porzio Catone RM, Italy
[6] Advanced Research Computing, University of Birmingham, United Kingdom, B15 2TT
[7] INAF – Osservatorio Astrofisico di Catania, Via S. Sofia, 78, 95123 Catania, Italy
[8] Department of Physics and Astronomy, Aarhus University, Ny Munkegade 120, DK-8000 Aarhus C, Denmark
[9] GRANTECAN, Cuesta de San José s/n, E-38712 Breña Baja, La Palma, Spain
[10] Instituto de Astrofísica de Canarias, E-38205 La Laguna, Tenerife, Spain

**ABSTRACT**

*Context.* Red giants displaying solar-like oscillations allow precise model-dependent stellar properties to be derived. Asteroseismic binaries, which are rare binaries with two such oscillators, allow us to further study coeval stars together as one.
*Aims.* We investigated a sample of red giants that have photometric or asteroseismic indications of binarity, in order to confirm their binary nature. We then sought to investigate the impact of simultaneously modeling two oscillators of an asteroseismic binary.
*Methods.* We derived indicators of binarity from high-resolution spectroscopy. We then used individual mode frequencies to infer stellar properties for; one binary that was not formed in the Milky Way and; three asteroseismic binaries with red-giant-branch stars.
*Results.* We confirm 13 of our 37 candidate systems as spectroscopic binaries, 8 of which are seismic binaries as well. For two additional candidates, KIC 6501237 and 11299484, we used asteroseismic modeling to confirm that the stellar components are coeval.
*Conclusions.* We confirm binarity in 10 asteroseismic binary candidates, which is the first step needed to use asteroseismic binaries as benchmark and calibration stars. We demonstrate that seismic binaries with two red-giant-branch stars can be used to infer the stellar helium content to 3-4% precision. The metal-poor ex-situ binary KIC 2971380 hints for a need to correct the $\nu_{\rm max}$ scaling relation, supporting recent studies of extremely metal-poor oscillators. Finally, we remark that two asteroseismic binaries in our sample show indications of dipole mode suppression in the dimmest star, making them interesting targets for magnetic field study due to the additional constraints from the companion's oscillations.

**Key words.** (stars:) binaries: general – asteroseismology – stars: oscillations

## 1. Introduction

Asteroseismology of red giants (RG) with solar-like oscillations allow for precise inference of fundamental stellar parameters. For stars with long-baseline photometric monitoring as provided by the *Kepler* space mission (Borucki et al. 2010), inference using individual mode frequencies, in particular, can be used for Galactic archaeological study, as the stellar mass and age can be inferred with better than 2 and 10% precision, respectively (see, e.g., Montalbán et al. 2021; Thomsen et al. 2025). Asteroseismic modeling inferences rely on the use of stellar evolution models, and in order to benchmark the accuracy of these predictions, independent validators are needed. Binary stars containing a solar-like oscillator, particularly eclipsing binaries, have been shown as very suitable for this task (Brogaard et al. 2018, 2022; Themeßl et al. 2018; Thomsen et al. 2022, 2025). However, the sample size of suitable eclipsing binaries is currently limited, with less than two dozen having *Kepler* observations (Gaulme et al. 2016; Gaulme & Guzik 2019; Benbakoura et al. 2021). In the *Kepler* field, a few open clusters host oscillating RGs with detectable oscillations, along with independent constraints from eclipsing binaries and photometry (see, e.g., Brogaard et al. 2012, 2021, 2023; Handberg et al. 2017; Dufresne et al. 2026). However, their exploration of the mass-metallicity parameter space is lacking, and open and globular cluster constraints outside of the *Kepler* field are further limited by lower seismic quality (e.g. Miglio et al. 2016; Lund et al. 2016; Tailo et al. 2022; Howell et al. 2024, 2026; Stello et al. 2026).

This highlights the need for more stellar systems that can provide constraints for calibration of asteroseismology and stellar models. Asteroseismic binaries, which are binary systems where both stars show detectable oscillations, are a unique type of system that can fill the gaps left by other calibrators. These systems do not necessarily offer model-independent constraints on fundamental parameters. However, when the oscillators' mode frequencies are not overlapping, they can allow us to perform analysis of two coeval oscillators, typically at different luminosities and/or different evolutionary states. So far, only a few cases have been confirmed or studied as true binary systems (Appourchaux et al. 2015; White et al. 2017; Li et al. 2018; Beck et al. 2018; Marcadon et al. 2018; Murphy et al. 2021; Grossmann et al. 2025; Schimak et al. 2026), but many more candidate systems have been published or investigated through kinematics, photometry, and/or seismology (Tayar et al. 2015;

⋆ j.s.thomsen@pm.me

Themessl et al. 2018; Bell et al. 2019; Espinoza-Rojas et al. 2025, and Mazzi et al. in prep.). Through population synthesis including binary interaction modeling, Mazzi et al. (2025) estimated that 20 − 80 oscillating RGs in the *Kepler* field should be a detectable asteroseismic binary. Uniquely, Mazzi et al. (2025) predicted that practically all RG+RG asteroseismic binaries should not have interacted presently or in the past, typically on a wide orbit, and given the comparably short evolutionary timescale of the red-giant-branch and later RG stages, their initial masses should therefore be almost the same. When their current surface and interior structure differ from one another, the two sets of oscillations should in principle provide us with unique constraints on the "same" star, at two different parts of its evolution. Such constraints can rarely be obtained outside of clusters, but asteroseismic binaries can provide this across the age and metallicity span of the field stars.

The search effort for evolved asteroseismic binaries is still ongoing, with new techniques under development (see, e.g. Choi et al. 2025, for a study of how the complications from overlapping oscillations can be used as an indicator). Combining asteroseismic, astrometric, and photometric information in search of photometrically over-luminous stellar systems is particularly rewarding (Mazzi et al., in prep), because detection of the oscillations in the dimmer companion typically requires luminosity ratios that also favour detection of the dimmest star through photometric excess (Mazzi et al. 2025).

In this work, we present a spectroscopic follow-up of a sample of 37 candidates for binary systems, selected based on their seismology (candidate asteroseismic binaries) or based on photometric excess as evaluated by their seismology (Mazzi et al., in prep). For a subsample of confirmed binaries, we perform a detailed asteroseismic inference, including the fitting of both star's oscillation modes in the case of asteroseismic binaries.

In Sect. 2, we outline the details of the spectroscopic observing programme and target list. In Sect. 3, we summarise the analysis of spectral line broadening functions, which we used to quantify spectroscopic variability in our sample, which we use to confirm stars as spectroscopic binaries. We summarise the most interesting targets from the spectroscopic study in Sect. 3.2. In Sect. 4, we present a detailed asteroseismic analysis of four targets, KIC 2971380 and three asteroseismic binary candidates KIC 6501237, 10592924, and 11299484. This includes peakbagging of the individual oscillation mode frequencies, as well as an asteroseismic modeling inference based on the radial mode frequencies. Finally, we summarise and conclude in Sect. 5

## 2. Spectroscopic observations

We performed spectroscopic follow-up observations of select binary candidates with the high-resolution ($R \sim 67.000$, $\delta v \sim$ 4.5km/s) spectrograph FIES at the Nordic Optical Telescope (Telting et al. 2014), in order to confirm them as spectroscopic binaries. With our observational strategy, we aimed to obtain at least two spectra with a long baseline, for as many stars as possible, and to follow up with more epochs on the most promising candidate binary systems. This observing proposal was run with filler time status, which meant that observations were only fitted into the observing queue on nights with scheduling gaps. For this reason, we kept the exposure times short, thereby prioritising RV measurement and investigation of the average line profile. The Signal/Noise of our observations was in general not high enough for detailed photospheric analysis of our targets. The selection of targets was an ad-hoc mix between several sources of candidate systems. We included a subsample of targets from the following sources:

- An early version of a photometric-asteroseismic binary candidate catalogue based on Willett et al. (2026). This catalogue will be presented in Mazzi et al. (in prep.).
- A sample of asteroseismic oscillators with poorly fitting single star background fits, which we confirmed to stem from a second oscillator in the power spectrum (priv. comm., Josefina Montalbán).
- A sample of double-oscillators that we found by manually investigating the KEPSEISMIC power spectra.
- Additional targets from the samples of candidate systems presented in Colman et al. (2017); Bell et al. (2019); Gaulme et al. (2020); Schonhut-Stasik et al. (2020).

## 3. Broadening function analysis

To investigate binarity, we aimed to derive spectroscopic measures of variability in the average line profile, both due to changes in Doppler shift (RV variability) and changes in the line profile (indicative of two stellar components with RV variation). We first performed dimensionality reduction on the spectra by calculating the average line broadening function (BF) (Rucinski 1999) of each spectrum. We used a fixed sharp-line synthetic template spectrum for all stars from Coelho et al. (2005), with $T_{\rm eff}$ = 4750K, $\log g$ = 2.5, [Fe/H] = 0.0, and [$\alpha$/Fe] = 0.0, and limited the calculation to the optical region 4500 − 5825Å to avoid telluric lines and interstellar Na in the observations, as well as low-Signal/Noise (S/N) in the blue. We further smoothed the BFs with a Gaussian kernel having $\sigma$ = 1km/s to reduce regression-induced noise from the wavelength-to-velocity transformation.

The BF is the least-squares profile that the sharp-line template must be convolved with to reproduce the observations, and it is therefore a best-fit representation of the average shape and Doppler-shift of the spectral lines, when compared to the template. Large asymmetries, bimodality, as well as changes in BF shape and RV over time can be indicators of binarity, which can be explored with model profile fitting. A static but bimodal BF can also indicate a chance alignment of two stars not resolved by the spectroscopic follow-up, but this can require a long time baseline to confirm unless the stars are well-separated in RV.

In order to quantify spectroscopic binarity of the targets, we performed model fits to the BF of each spectrum. we used a Gaussian model. With this fit we assumed that the target is single-lined and not significantly broadened by rotation. The latter is a reasonable assumption for most RGs, because the line profile is often dominated by instrumental broadening due to slow surface rotation. The Gaussian model is:

$$f_{\rm Gauss}(v) = \frac{a}{\sigma\sqrt{2\pi}} e^{\frac{(v-rv)^2}{2\sigma^2}}, \quad (1)$$

with $a$ and $\sigma$ being the amplitude and standard deviation of the Gaussian function, while $v$ is the velocity bin and $rv$ is the RV center of the Gaussian.

For parameter fitting and uncertainty estimation, we used non-linear least squares optimisation. The fitted-parameter uncertainties are formal least-squares estimates, whose reliability depends on the uncertainties assigned to the input BF values. We estimated the uncertainty of the BF data from the variance outside of the line profile.

KIC 2971380 is one of several clearly variable SB2 systems, and the only one that we observed for more than one orbit. We

had enough observing epochs to perform a precise RV extraction for all the spectra, despite several of them having overlapping line profiles. We illustrate this in Fig. 1. We used a model with two Gaussian profiles, and fitted the eight BFs simultaneously, to enforce the same line widths and amplitude ratios. We performed a linear least squares fit within the non-linear optimisation, in order to marginalise out the continuum and absolute amplitude of each BF. This way, the non-linear optimisation had $3+2n$ free parameters ($A_2/A_1$, $\sigma_1$, $\sigma_2$, $n \times rv_1$, and $n \times rv_2$), where $n$ is the number of spectra. For a few other stars (see Table A.1), a similar SB2 fit helped confirm binarity, despite not being sufficient for constraining the orbital motion. For KIC 2971380, the number of spectra also allowed us to fit the orbital motion directly to the BFs, which gave a similar result to that of first extracting the RVs, and then fitting the orbit.

The data in the BFs is not normally distributed, but includes a significant level of correlation (see Fig. 1). Some of this correlation is systematically induced, due to mismatches between the features of the template and the observed spectrum. However, the majority part comes from the transformation of a noisy spectrum from wavelength to velocity space (see Rucinski 1999). This can also be considered overfitting noise, since it is amplified by the size of the BF design matrix. We have attempted to dampen this noise through smoothing with a Gaussian filter having $\sigma$ = 1km/s. This reduces the amplitude, but also imprints an additional correlation between the velocity bins. For KIC 2971380, we explored the impact of the total correlation on the output uncertainties. We assumed that the residuals follow a multivariate normal distribution with a stationary covariance, that is, one which is dependent only on the velocity difference between two bins, and not the absolute velocity. We approximated this covariance matrix by calculating the autocorrelation function of the residuals, after a best-fitting BF model was subtracted. We found that the resulting orbital parameters and uncertainties of KIC 2971380 are not significantly different from that obtained when neglecting this correlation. The output parameters for KIC 2971380 presented in this work were calculated including this contribution. However, based on these findings we have neglected the correlation for the targets in the sample that have less spectra, in order to preserve computational efficiency.

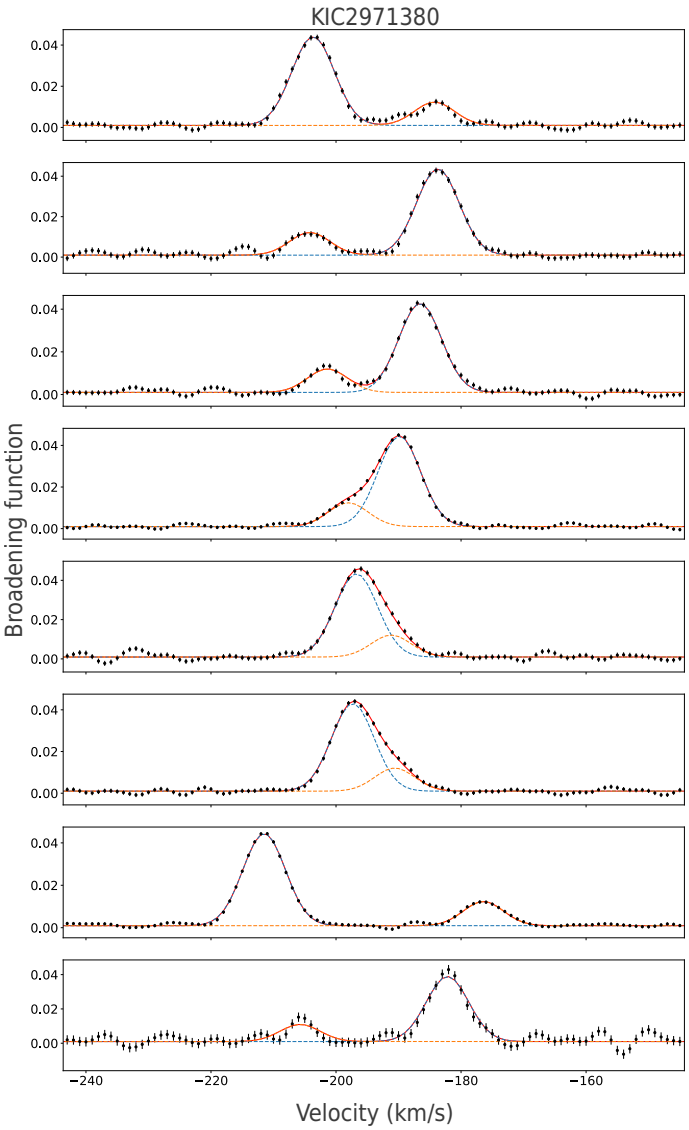


**Fig. 1.** Simultaneous double-Gaussian fit to the BFs of all spectra of KIC 2971380. The combined model is shown in red, while orange and blue dashed lines are the two components.

### 3.1. Binary indicators

Below, we detail the flags used to indicate binarity. We observed 37 stars with observations over at least two nights. For these stars, we explored if variations were detectable in the BF. These are summarised in Table A.1 in the appendix. The measures quoted in the table are outlined below.

**Slope $\frac{dv}{dt}$:** We estimated the RV variation by performing a linear fit of the RVs as a function of time, thereby assuming that the candidate binary has a period significantly longer than the baseline. The slope $dv/dt$ gives an indication of drifts in the RV over long timescales.

**Slope fit ΔBIC:** We also tested the fit quality of the above line fit against a constant fit, by comparing the Bayesian information criterion (BIC) of both. Negative ΔBIC means that the line fit was preferred over the constant.

**RV scatter $\Delta v$:** We independently estimated the RV variation, as the combination of the two RV measurements with highest significant difference relative to their combined uncertainty.

**Change in width $\Delta\sigma$:** We made an estimate of the most significant variation in Gaussian width $\sigma$, obtained by fitting a single Gaussian profile to the BF.

For the RV calculations, we have added 50 m/s in quadrature to all RV uncertainties, to account for potential instrumental drift or astrophysical variability in the line profile.

For ten of the 37 systems, the BF profile was visually bimodal. We therefore fitted a combination of two Gaussians, with the same method as described for KIC 2971380 in Sect. 3. We verified that these two-profile models had a better BIC than a one-profile fit. For these 10 systems, the velocity values reported in Table A.1 refer to the separation $RV_2 - RV_1$, rather than the absolute velocities. For example, the parameter $v$ is the most significant difference of all the measurements of $|RV_2 - RV_1|$. These double-lined measurements are independent of any potential drift in the instrumental zero-point, but they can still have astrophysical variation in the line profile from e.g. stellar spots.

In order to report a star as significantly variable in Table A.1, we required that either ΔBIC $< -10$, time variation in the width ($\Delta\sigma > 4 \cdot \mathrm{Err}(\Delta\sigma)$), or in the velocity ($\Delta v > 4 \cdot \mathrm{Err}(\Delta v)$). A few stars show tentative indications of binarity, either $\Delta\sigma/\mathrm{Err}(\Delta\sigma) \sim 2-4$, or both the slope and $\Delta v$ larger than the uncertainty. In particular, KIC 11299484 shows a clearly bimodal line profile,

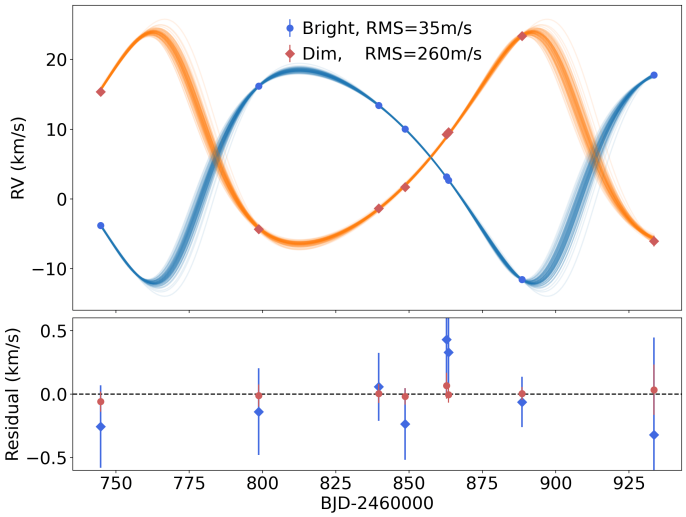


**Fig. 2.** Measured radial velocities for KIC 2971380, including a fit for the orbital parameters. RVs are offset by +200 km/s.

but the RV variation is only at the $1\sigma$ significance level over a baseline of 255 days.

### 3.2. Binary systems

In this section we present specific details and analysis for some of the systems whose binary nature we can either confirm, tentatively indicate as binaries, tentatively disprove, and one system, KIC 6369592, that we can conclusively disprove as a binary.

#### 3.2.1. KIC 2971380

A low-luminosity RGB star with an observed asteroseismic period spacing of $\Delta P = 70.84 \pm 0.03$ (Mosser et al. 2018). This target has previously been studied in detail with asteroseismology, as its photospheric chemical composition and Galactic kinematics support an ex-situ origin, likely from Gaia Enceladus (Montalbán et al. 2021; Borre et al. 2022). With our spectroscopic follow-up we confirm it as an SB2 system with a luminosity ratio around 25%, based on the BF amplitudes. We performed a fit to the radial velocities and confirm that the mass ratio is statistically consistent with unity at 1% precision, suggesting that the companion is likely evolved past the main sequence as well. The power spectrum does not show indications of oscillations from the dimmer companion.

#### 3.2.2. KIC 4260884, 7697607, 8479383, 10592924

These are asteroseismic binaries with separated oscillation envelopes. We have indications of them being spectroscopic double-lined binaries with RV variation. KIC 8479383 contains at least one core-Helium burning (CHeB) star, as evidenced by the star's mixed modes. KIC 7697607 has two oscillators with a small separation in $\nu_{\rm max}$, which means that the oscillation envelopes partially overlap for at least one radial order. The power spectrum of KIC 10592924 presents two RGB stars with high quality oscillations. The dimmest star shows a strong suppression of its dipole mode amplitudes.

KIC 4260884 has well-separated oscillations for the two stars. We measured $\nu_{\rm max} = 47.1 \pm 1.4\mu$Hz and $\Delta\nu_{\rm obs} = 4.448 \pm 0.017\mu$Hz for the brighter star, and $\nu_{\rm max} = 110.2 \pm 4.2\mu$Hz and $\Delta\nu_{\rm obs} = 9.310 \pm 0.021\mu$Hz for the dimmer star. $\nu_{\rm max}$ was measured from a double-Gaussian background fit with two super-Lorentzian (Kallinger et al. 2014) profiles, while $\Delta\nu_{\rm obs}$ was obtained by first peakbagging the modes (see Sect. 4.1 for the method), and then fitting the observed asymptotic relation (Mosser et al. 2013). With $T_{\rm eff} = 4875 \pm 120$K from APOGEE DR17 (adopted 120K uncertainty), the uncorrected scaling relation mass of the brighter star is $2.33 \pm 0.23 M_\odot$. The power spectrum of KIC 4260884 is generally "noisy", particularly for the brightest star, which shows a low small frequency separation $\delta\nu_{0,2}$ relative to the width of the Lorentzians describing the stochastically driven pressure-dominated modes. The modes of the bright star do not present a clear CHeB mixed mode pattern, but appear similarly complex and broadened. The RGB phase is relatively short-lived for stars of this mass, and there is therefore the possibility that this star is either in the late CHeB or early asymptotic-giant-branch phase.

**Table 1.** Properties of KIC 2971380 obtained from spectroscopic orbit modelling.

| | |
|---|---|
| $\frac{\rm Mass_{dim}}{\rm Mass_{bright}}$ | 1.005 (10) |
| $M_{\rm bright} \sin^3 i\ (M_\odot)$ | 0.170 (11) |
| $M_{\rm dim} \sin^3 i\ (M_\odot)$ | 0.71 (11) |
| $a \sin i\ (R_\odot)$ | 75.1 (17) |
| RV semi-amplitude $K_{\rm bright}$ (km/s) | 15.28 (30) |
| RV semi-amplitude $K_{\rm dim}$ (km/s) | 15.20 (34) |
| Eccentricity $e$ | 0.2643 (47) |
| Periastron longitude $\omega$ (°) | 222.4 (42) |
| Orbital period (days) | 129.26 (33) |
| $t_{0,\rm peri}$ (days)[a] | 1030.2 (26) |
| RV zero-point $\gamma_{\rm bright}$ (km/s) | -193.82 (22) |
| RV zero-point $\gamma_{\rm dim}$ (km/s) | -194.22 (24) |

[a] Barycentric Julian date minus 2460000.

#### 3.2.3. KIC 6501237

There are two stars within 3" on-sky, with $\Delta G = 2.3$, with a parallax-derived line-of-sight separation of $0.03 \pm 0.6$pc, and Galactocentric velocity difference of only $\sim 2$ km/s. These stars were flagged by (Espinoza-Rojas et al. 2025) as having a bound-binary configuration probability of 50%. We have two spectra of the brightest star, taken $\sim$ 150 days apart, showing a small change in its RV and width. Unfortunately, one of the spectra was taken with observational seeing of 2", and likely contains a contribution from both stars, which can explain the RV variation. Given their close proximity and low RV difference, it is plausible that they are either in a bound orbit or in a close association. In Sect. 4, we treat them as a coeval pair, in order to explore if we can obtain a good asteroseismic double-star model fit under this assumption. A seismic confirmation would be interesting as Miglio et al. (2014) predicted that effectively all resolved asteroseismic binary candidate systems should be false positives, that is, chance alignments.

#### 3.2.4. KIC 5300269, 8479182, 8649099

These stars have a photometric excess, when an asteroseismic estimate of the intrinsic luminosity is compared with the apparent magnitude and Gaia DR3 derived parallax-distance (Mazzi et al, in prep.). They furthermore show complicated oscillation envelopes that could indicate the presence of two oscillators overlapping in the power spectrum. This hypothesis might be in-

vestigated in more detail with techniques such as those demonstrated in Choi et al. (2025). KIC 5300269 shows a change in BF shape over ∼ 120 days, which indicates the presence of two sets of spectral lines. Its *Kepler* light curve contains sinusoidal-like variability, which could be an indication of a rotational signal (spots). The star has been studied in Gaulme et al. (2020); Gehan et al. (2024) for this reason, where they concluded that it did not have significant indications of activity.

KIC 8479182 and KIC 8649099 both have photometric luminosities and APOGEE DR17 temperatures that put them at $\sim 2 \times L_{\rm RC}$. We confirm them both as double-lined and RV variable with our spectroscopic follow-up. These are expected to be the most prevalent asteroseismic binary of the *Kepler* red giants (Mazzi et al. 2025).

#### 3.2.5. KIC 5978324

KIC 5978324 is confirmed as an SB1 with our spectroscopic measurements, as well as with Gaia data (see Beck et al. 2024). The star was studied in Crawford et al. (2024, 2025) as part of a sample of the 48 most massive solar-like oscillators observed by *Kepler*, where they found $M = 4.7 \pm 0.3 M_{\odot}$. To date not many oscillating RG binaries in the $4 - 5 M_{\odot}$ range have been studied in detail from observations, and with clear binarity this target is therefore of potential interest, as it is near the mass where evolved stars show Cepheid pulsations during part of its evolution.

#### 3.2.6. KIC 6369592

Both the power spectrum and spectroscopic follow-up show two stars, but the $\nu_{\rm max}$ ratio of $0.516 \pm 0.006$ and BF integral ratio of $\sim 0.1 - 0.2$ give discrepant indicators for the luminosity ratio. The amplitude ratio of the two asteroseismic oscillation envelopes of $0.218 \pm 0.011$ support the luminosity ratio estimated from spectroscopy, suggesting that the spectroscopic lines match the two oscillators detected in the power spectrum. The RV separation of $21.2 \pm 0.1$ km/s is not seen to vary over 400 days, which confirms that the two stars cannot be in a gravitationally bound binary system. The large RUWE value and negative parallax from the Gaia data could indicate that the stars are partially resolved by Gaia, despite not having been identified as such by the pipeline. With new data in the upcoming Gaia DR4, this system might be resolved with the second star receiving its own identifier.

#### 3.2.7. KIC 5015647

This system shows very high RV variation (19 km/s per year) based on the two spectra taken 141 days apart. Its *Kepler* power spectrum presents a complicated solar-like oscillation pattern at $\sim 30 \mu$Hz, with a forest of narrow modes. In addition, the power spectrum contains a set of higher-amplitude, coherent peaks from $180 \mu$Hz until the nyquist frequency. The nearby source (8") KIC 5015657 (Gaia DR3 2053253684738428928) has a magnitude difference of only ∼ 2 in the Gaia G band. While it is clear from the spectroscopy that KIC 5015647 is a binary system, it should be investigated if the nearby source is the cause of one of the two signals in the power spectrum.

#### 3.2.8. KIC 4637699, 9412408, 11299484

These show two well-separated oscillators in their power spectra, and our RV measurements show marginal detections of variability. Particularly, KIC 11299484 clearly presents two spectral lines as well. These systems should be monitored over a longer baseline in order to confirm their RV variability.

#### 3.2.9. KIC 9392647/50

KIC 9392647 and 9392650 appear to be a chance alignment of two oscillators on the sky, as also found by Espinoza-Rojas et al. (2025). They found that the spectroscopic constraints of both stars from Gaia were compatible with the $\nu_{\rm max}$ of the two stars. The amplitude ratio of the two oscillation envelopes are different for the two stars' KEPSEISMIC power spectra, which indicates that the ratio depends on which pixels are included in the aperture photometry. Therefore, the oscillations belong to the two different resolved stars on the sky.

Although KIC 9392647 and 9392650 have nearly the same distance and sky position, their kinematics rule out a bound configuration. Their RVs differ by $\sim 40, \mathrm{km, s^{-1}}$, and their proper-motion difference of $\sim 6.6, \mathrm{mas, yr^{-1}}$ corresponds to $\sim 62, \mathrm{km, s^{-1}}$. In comparison, their angular separation of $6.2 \pm 0.012, \mathrm{arcsec}$ implies a projected separation of at least $\sim 11400, \mathrm{AU}$, for which the escape velocity is only of order $500, \mathrm{m, s^{-1}}$. The relative velocity is therefore far too large for the two resolved stars to be gravitationally bound.

An unresolved companion to one of the stars could in principle shift one measured RV away from the systemic velocity. However, a companion capable of producing an offset of tens of $\mathrm{km, s^{-1}}$ would leave a clear signature, either through an inflated Gaia RUWE or through a larger RV change between our two spectra. We therefore interpret KIC 9392647 and KIC 9392650 as a chance alignment rather than a bound pair.

However, we still detect minor RV variability for the lines of both stars. We have not identified the cause of this, but it could be either due to instrumental drift[1] or intrinsic variability (Hekker et al. 2008).

## 4. Asteroseismic inference of binaries

In this section, we present detailed peakbagging and asteroseismic inference of one ex-situ (accreted) Galactic binary for which we measured a radial velocity orbital solution in Sect. 3, and a proof-of-concept seismic investigation for three asteroseismic binaries, with the aim of using the oscillations of both stars.

### *4.1. Oscillation frequency measurement*

To measure the observed oscillation frequencies in the KEPSEISMIC power spectra (e.g. Pires et al. 2015, and references therein), we performed peakbagging by fitting a Lorentzian profile to each observed radial ($l = 0$), dipole ($l = 1$), and quadrupole ($l = 2$) mode. The aim was to accurately measure the radial mode frequencies for asteroseismic inference, and in cases where dipole modes were challenging to model with a single Lorentzian profile, we excluded them from the fit.

First, we fitted an asteroseismic background and power excess with DIAMONDS (Corsaro & De Ridder 2014) to capture granulation, oscillation power excess, and white noise

[1] see https://www.not.iac.es/instruments/fies/devel/FIES_drift_report.pdf

$W$. For the granulation, we used two super-Lorentzian profiles (Kallinger et al. 2014), and for the asteroseismic binaries KIC 6501237 and 10592924, we implemented a model to handle two Gaussian power excesses:

$$\mathcal{P}(\nu) = \eta(\nu)\left[\sum_{k=1}^{2}\left(\frac{2\sqrt{2}\sigma_k^2}{\pi\nu_k\left(1+\left(\frac{\nu}{\nu_k}\right)^4\right)}\right)+\sum_{j=1}^{2}\left(H_{\mathrm{osc},j}e^{-\frac{(\nu-\nu_{\max,j})^2}{2\sigma^2_{\mathrm{osc},j}}}\right)\right]+W, \tag{2}$$

$$\eta(\nu) = \mathrm{sinc}\left(\frac{\nu}{2\nu_{\mathrm{nyquist}}}\right)^2. \tag{3}$$

We attempted to include more granulation terms to match both stars in the asteroseismic binaries, but the power spectra did not contain enough information to constrain these independently.

After background fitting, we performed peakbagging of KIC 2971380 with DIAMONDS. The $\ell = 1$ modes had a well-resolved mixed mode characteristic, and we therefore fitted the individual mixed modes with narrow Lorentzians as well. The mixed modes do not appear like fully unresolved sinc profiles, but have a narrow but Lorentzian-like profile, indicative of a long but finite lifetime.

For the asteroseismic binaries, we manually peakbagged the oscillation modes using the affine-invariant Markov-Chain Monte Carlo (MCMC) sampler EMCEE (Foreman-Mackey et al. 2013). This manual fit was necessary as current automatic peakbagging codes (e.g. PBJam, DIAMONDS, FAMED Nielsen et al. 2021; Corsaro & De Ridder 2014; Corsaro et al. 2020) are not designed to handle two oscillation envelopes. Similar to the background fit, for the peakbagging we also accounted for the impact of the integration time on the oscillation amplitude. When evaluating the likelihood, we assumed that the noise characteristics of the power spectrum follows a $\chi^2$ distribution with two degrees of freedom.

The individual oscillation frequencies are reported in Table. C.1. The observed $\ell = 1$ modes of KIC 2971380 are reported in Table C.2. In addition to this, we measured the large frequency separation between radial orders $\Delta\nu_0$ (Table 2), by performing a linear fit of the radial mode frequencies, weighing the modes by the inverse of the observed variance. The reported uncertainties for $\Delta\nu_0$ are only the formal uncertainties. We also used the observed asymptotic relation of Mosser et al. (2011, 2013) to measure $\Delta\nu_{\mathrm{obs}}$, small frequency separation $\delta\nu_{\mathrm{obs},02}$, offset $\epsilon_{\mathrm{obs}}$, and curvature $\alpha_{\mathrm{obs}}$. Specifically, we used the relation

$$\nu_{n,l} = \left(n + \epsilon_{\mathrm{obs}} + (\alpha_{\mathrm{obs}}/2)\left(n - \frac{\nu_{\max}}{\Delta\nu_{\mathrm{obs}}}\right)^2\right)\Delta\nu_{\mathrm{obs}} \quad + \delta_{\mathrm{obs},0l}. \tag{4}$$

Here, we sampled the probability distribution with MCMC, including the observed $\nu_{\max}$ (with uncertainty). We furthermore included a nuisance parameter $\sigma_{\mathrm{jitter}}$ to account for intrinsic scatter, inflating the uncertainties by $\sigma = \sqrt{\sigma^2_{\mathrm{obs}} + \sigma^2_{\mathrm{jitter}}}$, since the detailed structure of the modes is neither reflected in the asymptotic relation nor in the observational uncertainty. This in general resulted in significantly higher parameter uncertainty estimates. The quoted uncertainties for $\Delta\nu_{\mathrm{obs}}$ in Table 3 are therefore more realistic than those reported for $\Delta\nu_0$.

### 4.2. Asteroseismic modeling inference

We performed an asteroseismic inference using a grid of stellar models with calculated theoretical oscillation frequencies. We used the alpha-version of AIMS3[2], which is a partial re-implementation of the Bayesian inference code AIMS (Asteroseismic Inference on a Massive Scale, Rendle et al. 2019). AIMS3 allowed us to define a likelihood function including two stars, whereas we could only study one star at a time in the the previous version. For mode identification, we used the older version of AIMS, since this was not reimplemented in AIMS3.

We used a grid of stellar evolutionary tracks and theoretical frequencies calculated with MESA version 11701 (Paxton et al. 2011; Paxton & et al. 2013, 2015, 2018, 2019) and GYRE (Townsend & Teitler 2013). This grid will be presented in full detail in Tailo et al. (in prep.), but it has already been tested on the eclipsing binary KIC 10001167 (Thomsen et al. 2025). Each model was evolved from the pre-main-sequence until the first thermal pulse. However, we restricted the grid to the RGB phase when fitting. The full grid spans; [Fe/H] from -2.0 to +0.55 with typical step of 0.25, with solar mixture from Asplund et al. (2009); [$\alpha$/Fe] from -0.2 to 0.4 in steps of 0.2; initial helium abundance $Y_i$ from 0.22 to 0.34 in steps of 0.03; and masses from 0.6 to 1.8 in steps of 0.05 $M_\odot$, and with additional models at mass $2.0, 2.15, 2.3, 2.45, 2.75, 3.0 M_\odot$. The atmosphere description by Krishna Swamy (1966) was used, and we included microscopic diffusion. Further choices regarding equation of state, opacities, and mixing were the same as in Miglio et al. (2021). The mixing-length-theory (MLT) was chosen to describe convection with the formula from Cox & Giuli (1968), and $\alpha_{\mathrm{MLT}} = 2.2902$ was obtained by solar calibration.

As observational constraints in AIMS3, we used only the radial mode oscillation frequencies and the frequency of maximum oscillation power, together with the observed surface iron abundance [Fe/H] from APOGEE DR17 (Abdurro'uf et al. 2022), combined with the alpha-enhancement [$\alpha$/Fe] in the format $(Z/X)_{\mathrm{surf}}$. We convert from [Fe/H] and [$\alpha$/Fe] to $Z/X$ with:

$$(Z/X)_{\mathrm{surf}} = (Z_\odot/X_\odot)\cdot 10^{[\mathrm{M/H}]}, \tag{5}$$

$$[\mathrm{M/H}] = [\mathrm{Fe/H}] + A, \tag{6}$$

$$A = \log_{10}(a\cdot 10^{[\alpha/\mathrm{Fe}]} + b), \tag{7}$$

$$a = 0.6387, \tag{8}$$

$$b = 0.3613. \tag{9}$$

The [M/H] calculation is based on the Salaris et al. (1993) correction, using the Asplund et al. (2009) solar mixture. Since all the stars we analysed are in binary systems, we only apply the metallicity constraint on the brightest star. The metallicity could be biased by dilution from the companion and blending of the lines of the two stars. We therefore adopted a conservative estimate for the uncertainty on the metallicities (0.1 dex). In Sect. 4.3, we confirm that the expected bias on the spectroscopy from the presence of two overlapping sources is less than this, for our targets.

We corrected for the theoretical frequencies using the cubic (one-term) prescription of Ball & Gizon (2014), with a correction for each star. These are included as additional sampling parameters. In some cases, the fit quality was much better when using the two-term prescription of Ball & Gizon (2014), including an inverse term (see also Jørgensen et al. 2021, , for a detailed investigation). The two-term prescription is

$$\delta\nu_{\mathrm{surf}}(\nu, \mathcal{I}) = \left[a_{-1}(\nu/\nu_{\mathrm{ac}})^{-1} + a_3(\nu/\nu_{\mathrm{ac}})^3\right]/\mathcal{I}, \tag{10}$$

while the cubic (one-term) prescription excludes the $a_{-1}$ term. Here, $\nu$ is a theoretical mode frequency, $\nu_{\mathrm{ac}}$ is the acoustic cut-off frequency, and $\mathcal{I}$ is the normalised mode inertia. As proxy

[2] https://gitlab.com/warrickball/aims3-alpha

of $\nu_{\rm ac}$, we used the model $\nu_{\rm max}$. Since $\nu_{\rm ac}$ and $\nu_{\rm max}$ are approximately proportional (Brown et al. 1991; Belkacem et al. 2011), this replacement simply results in an offset in $a_3$ and $a_{-1}$.

We defined a logarithmic likelihood function comprised of the following $\chi^2$ terms for the bright (bri) and dim stellar components in the asteroseismic binaries:

$$-\ln\mathcal{L} \propto \chi^2_{\mathrm{bri},\ell=0} + \chi^2_{\mathrm{dim},\ell=0} + \chi^2_{\mathrm{bri},\nu_{\rm max}} + \chi^2_{\mathrm{dim},\nu_{\rm max}} + \chi^2_{\mathrm{bri},(Z/X)}, \quad (11)$$

$$\chi^2_{\ell=0} = \sum_n \frac{(\nu_{n,0} - (\nu_{n,0\,\mathrm{model}} + \delta\nu_{\mathrm{surf}\,n,0}))^2}{\sigma^2_{n,0}}, \quad (12)$$

$$\chi^2_{\nu_{\rm max}} = \frac{(\nu_{\rm max} - \nu_{\mathrm{max,\,model}})^2}{\sigma^2_{\nu_{\rm max}}}, \quad (13)$$

$$\chi^2_{(Z/X)} = \frac{((Z/X)_{\rm surf} - (Z/X)_{\mathrm{surf,\,model}})^2}{\sigma^2_{(Z/X)_{\rm surf}}}. \quad (14)$$

With this likelihood, we do not include any relative weighing of the "classical" and "seismic" constraints, since our only non-seismic constraint is the metallicity, which is only conservatively constrained with an uncertainty of 0.1dex on [Fe/H].

For sampling the likelihood, we used MCMC with EMCEE (Foreman-Mackey et al. 2013). We used an RGB subgrid of the MESA grid, with fixed [$\alpha$/Fe] = 0.0 for the asteroseismic binaries, and [$\alpha$/Fe] = 0.15 for KIC 2971380. We sampled the following stellar parameters: Mass of the brightest star, mass ratio of the binary, shared metallicity [Fe/H], shared initial helium fraction $Y_i$, and a-dimensional age $\tau$ (one for each star). We define $\tau$ as the mass of the helium core, which is a feature that increases monotonically with real age $A$ during the full RGB. We used $\tau$ in place of the real age, both for sampling and interpolation, in order to reduce the occurrence rate of interpolation failure during sampling. Interpolation failure happened frequently when one of the several tracks involved in the grid interpolation did not have a model with the correct age. As outlined in Rendle et al. (2019), this is a common problem when interpolating grids of stellar models, because the age correlates with the other grid parameters. For seismic inference of evolved stars in particular, the real age depends not just on the star's life past the main sequence, but also on the length of the main sequence. When the grid is cropped to exclude the main sequence, the interpolation can therefore frequently require a model that is off-grid. Using an a-dimensional proxy solves this problem. For our interpolation scheme, the real age is then just an output parameter, along with most of the other model parameters. We verified that this parameter transformation did not bias the likelihood sampling, since the logarithm of the Jacobian (the logarithm of the partial derivative $\ln(\partial\tau/\partial A)$) is well-approximated as locally constant relative to the overall gradient of the likelihood.

Since we use a stellar structure proxy for the age, we needed a free parameter for each star. We enforce coevality by including a Gaussian prior on the age difference of the stars, requiring that their ages agree within 5% of the mean age of the two stars (e.g. 250 Myr for 5 Gyr). This is roughly $50-90$% of the typical statistical uncertainty on age that we expect for a single RGB star with *Kepler* data on individual mode frequencies (see, e.g., Montalbán et al. 2021; Thomsen et al. 2025), and it is therefore not a particularly restrictive constraint. The agreement (or disagreement) between the posterior ages of the two stars, together with the seismic fit quality, can therefore be further informative of whether coevality is a good assumption.

### 4.3. Spectroscopic bias from two stars

Our spectroscopic observations from FIES are too low Signal/Noise to be used for accurate atmospheric analysis. However, many of our targets have also been observed at lower spectroscopic resolution ($R \sim 22.500$, $\delta v \sim 13$ km/s) in the near-infrared by APOGEE (Majewski et al. 2017), and have atmospheric parameters available in APOGEE DR17 (Abdurro'uf et al. 2022). These parameters were derived under the assumption that the source only contained a single star.

We here evaluate whether this assumption is sufficient to produce an accurate measure of atmospheric parameters for the brightest star, at least within typically adopted uncertainties for effective temperature and metallicity. Since the asteroseismic binaries have RV separations below the spectral resolution of APOGEE, we can safely assume that both stars contribute to the lines used for atmospheric analysis. For the 3" resolved system KIC 6501237, whether the companion was included in the observations or not likely depended on the nightly seeing, and this investigation therefore represents an upper limit to the expected bias.

We used the metallicity from APOGEE DR17, together with the luminosity ratio, effective temperatures, and logg's of both components that we inferred asteroseismically (see Table 3). We then constructed synthetic spectra with the relevant atmospheric parameters, and blended them using the luminosity ratio. Here, we neglect the chromatic impact on the light ratio, which is sufficient since the temperature ratio is close to unity. In Fig. 4, this averaging is illustrated in the near-infrared for KIC 10592924. From this, we conclude that the true metallicity is likely within 0.1 dex of the observed, and the temperature of the brightest star is expected to be within 150K of the observed. Since KIC 10592924 has the most equal luminosity ratio, particularly when compared to the difference in effective temperature between the stars, the bias is expected to be smaller for KIC 6501237 and KIC 2971380.

### 4.4. Inference results

The asteroseismic inference based on radial mode frequencies generally converged to a single solution for all three binaries. The results of our seismic inferences are summarised in Table 3.

#### 4.4.1. The ex-situ binary, 2971380

The oscillations of KIC 2971380 are shown in Fig. 3, together with the fit result of our seismic modeling inference. The power spectrum of KIC 2971380 only has detectable oscillations for the bright component. From seismic inference, we are able to constrain the mass of the brightest star. When combined with the RV orbital motion fit, we have inferred a stellar-model-dependent orbital inclination and semi-major axis of $35.43 \pm 0.94^\circ$ and $129.6 \pm 4.2 R_\odot$, respectively. The radius of the brightest star relative to the orbit is therefore $4.76 \pm 0.16$%. With the eccentricity of $0.264 \pm 0.005$, we should not expect binary interaction to have impacted the evolution of this star yet. As demonstrated in Montalbán et al. (2021), this system was most likely not formed in the Milky Way, but accreted later on. This is exemplified by its high Galactic eccentricity, but also by its APOGEE DR17 abundances; it has a relatively low $\alpha$ enhancement ([$\alpha$/Fe] = 0.15) for its metallicity ([Fe/H] = −0.77), as well as a low [Al/Fe] = −0.04 and high [Mg/Mn] = 0.50 (see, e.g., Das et al. 2020). Based on the binary orbital parameters, the system is similar to the thick disk benchmark eclipsing binary KIC 10001167 stud-

**Table 2.** Average asteroseismic parameters for four binaries. Uncertainties are given relative to the last reported digits.

| KIC | | 6501237 | 10592924 | 11299484 | 2971380 |
|---|---|---|---|---|---|
| **Asymp. fit (Bright)** | | | | | |
| $\nu_{\rm max}$ [a] | $\mu$Hz | 62.86 (19) | 52.52 (24) | 48.27 (23) | 77.63 (26) |
| $\Delta\nu_0$ | $\mu$Hz | 6.1538 (42) | 5.3827 (42) | 4.9899 (48) | 7.8457 (45) |
| $\Delta\nu_{\rm obs}$ | $\mu$Hz | 6.1822 (81) | 5.402 (11) | 5.056 (12) | 7.920 (14) |
| $\delta\nu_{\rm obs,02}$ | $\mu$Hz | 0.831 (29) | 0.743 (39) | 0.673 (39) | 1.115 (49) |
| $\epsilon_{\rm obs}$ | | 0.075 (14) | 0.084 (20) | 0.062 (22) | 0.131 (19) |
| $\alpha_{\rm obs}$ | | 0.0145 (16) | 0.0168 (24) | 0.0168 (33) | 0.0154 (27) |
| $\sigma_{\rm jitter}$ | $\mu$Hz | 0.046 (13) | 0.065 (18) | 0.059 (19) | 0.068 (22) |
| **Asymp. fit (Dim)** | | | | | |
| $\nu_{\rm max}$ [a] | $\mu$Hz | 123.18 (41) | 130.56 (82) | 89.82 (41) | |
| $\Delta\nu_0$ | $\mu$Hz | 10.4818 (77) | 11.0416 (76) | 8.1095 (86) | |
| $\Delta\nu_{\rm obs}$ | $\mu$Hz | 10.538(20) | 11.059 (15) | 8.154 (25) | |
| $\delta\nu_{\rm obs,02}$ | $\mu$Hz | 1.339 (52) | 1.436 (38) | 1.084 (44) | |
| $\epsilon_{\rm obs}$ | | 0.180 (22) | 0.246 (16) | 0.159 (34) | |
| $\alpha_{\rm obs}$ | | 0.0092 (33) | 0.0000 (22) | 0.0183 (63) | |
| $\sigma_{\rm jitter}$ | $\mu$Hz | 0.065 (24) | 0.049 (18) | 0.056 (28) | |

[a] From the background model fit. See text for details.

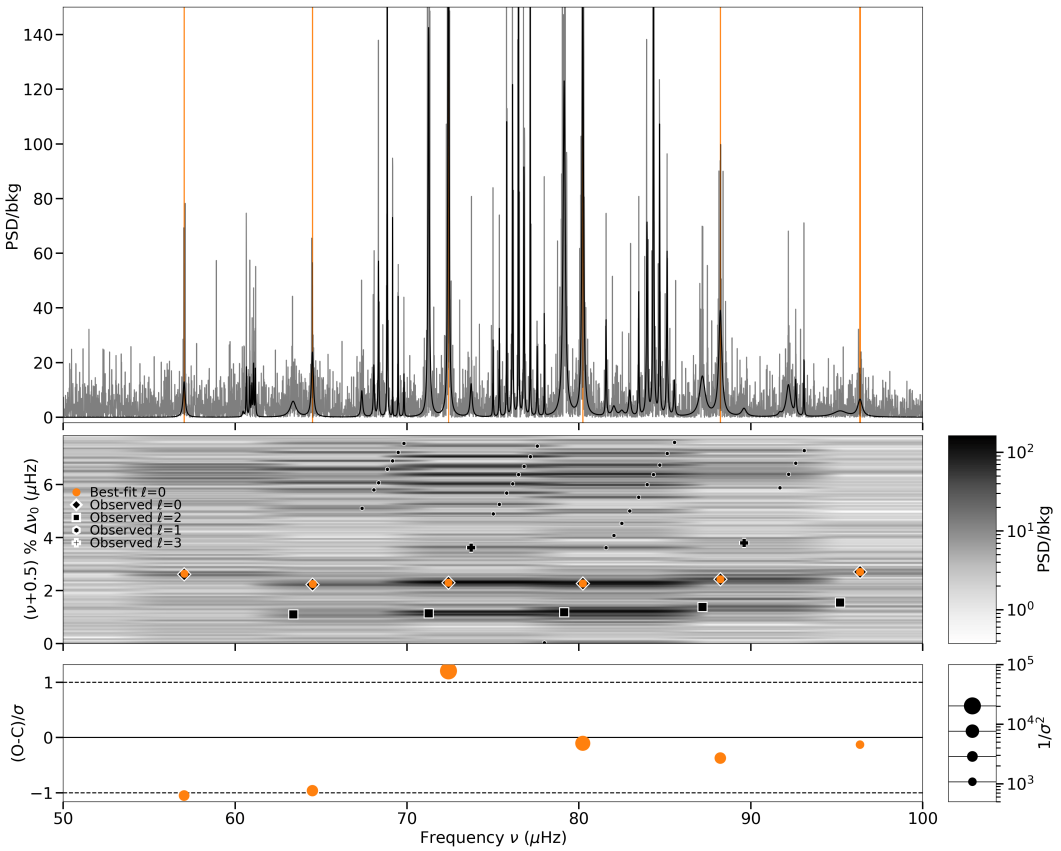


**Fig. 3.** Top: PSD of KIC 2971380 (grey), divided by the granulation background model. Includes best-fit peakbagging models of each oscillation mode (black). The 68% confidence interval of the radial mode frequencies are highlighted in orange. Middle: Échelle diagram (rotated), highlighting observed mode frequencies (black/white markers), and best-fit theoretical radial mode frequencies from the asteroseismic modeling inference (orange). Frequency uncertainty is included, but is often below the marker size. Bottom: Significance of the (Observed - Calculated) residuals for the radial mode frequencies, relative to the observation uncertainty. The marker size is scaled by the statistical weight assigned to each mode during the seismic inference. Dashed lines indicate $\pm1\sigma$ deviation.

ied in Thomsen et al. (2025), with a similar orbital period, eccentricity, and semi-major axis. It is worth mentioning that the seismically inferred age of KIC 2971380 places it at 11.7 ± 1.0 Gyr, which is 1.4 ± 1.1 Gyr ($\sim 1.2\sigma$) older than KIC 10001167. This is roughly similar to the age difference found between the two stars in Montalbán et al. (2021), who used the CLES stellar evolution code (Scuflaire et al. 2008), which indicates that the result is robust against model systematics.

For our analysis of KIC 2971380, we only included the metallicity and radial mode frequencies as observational constraints, excluding a constraint on $\nu_{\rm max}$. $\nu_{\rm max}$ is frequently coupled to the surface gravity $g$ through a solar scaling relation, which is derived under assumption that $\nu_{\rm max}$ is proportional to the acoustic cutoff frequency $\nu_{\rm cutoff}$ (Brown et al. 1991;

**Table 3.** Asteroseismic model inferences for three binaries, based on radial modes. Uncertainties are given relative to the last reported digits.

| KIC | | 6501237 | 10592924 | 11299484 | 2971380 |
|---|---|---|---|---|---|
| Input: $(Z/X)_{\rm surf,bright}$ [a] | | 0.0152 (35) | 0.0096 (22) | 0.0191 (44) | 0.0039 (13) |
| Input: $\nu_{\rm max,bright}$ | $\mu$Hz | 62.86 (19) | 52.52 (24) | 48.27 (0.23) | |
| Input: $\nu_{\rm max,dim}$ | $\mu$Hz | 123.18 (41) | 130.56 (82) | 89.82 (0.41) | |
| Input: [$\alpha$/Fe] | dex | 0.0 | 0.0 | 0.0 | 0.15 |
| Input: $M_{\rm dim}/M_{\rm bright}$ | | | | | 1.005 (10) |
| Input: $L_{\rm dim}/L_{\rm bright}$ | | | | | 0.25 (5) |
| $M_{\rm bright}$ | $M_\odot$ | 1.167 (21) | 1.223 (18) | 1.200 (18) | 0.871 (17) |
| $M_{\rm dim}$ | $M_\odot$ | 1.165 (20) | 1.215 (19) | 1.203 (19) | 0.865 (17) |
| $M_{\rm dim}/M_{\rm bright}$ | | 0.9980 (91) | 0.993 (10) | 1.001 (10) | 0.9940 (29) |
| [Fe/H] | dex | -0.10 (10) | -0.322 (78) | -0.038 (83) | -0.752 (86) |
| $Y_i$ | | 0.296 (11) | 0.2667 (84) | 0.2720 (86) | 0.25154 (89)[b] |
| $\rm Age_{bright}$ | Gyr | 4.65 (49) | 4.00 (32) | 5.47 (61) | 11.70 (99) |
| $\rm Age_{dim}$ | Gyr | 4.63 (52) | 4.03 (34) | 5.41 (62) | |
| $R_{\rm bright}$ | $R_\odot$ | 7.975 (56) | 8.930 (42) | 9.228 (48) | 6.167 (40) |
| $R_{\rm dim}$ | $R_\odot$ | 5.645 (35) | 5.562 (31) | 6.751 (38) | 2.80 (32) |
| $\log g_{\rm bright}$ | dex | 2.7020 (21) | 2.6238 (21) | 2.5871 (22) | 2.7981 (27) |
| $\log g_{\rm dim}$ | dex | 3.0012 (22) | 3.0320 (21) | 2.8595 (21) | 3.48 (10) |
| $\rho_{\rm bright}$ | $10^{-3}\rho_\odot$ | 2.301 (10) | 1.7173 (14) | 1.5265 (25) | 3.7151 (70) |
| $\rho_{\rm dim}$ | $10^{-3}\rho_\odot$ | 6.473 (25) | 7.0596 (78) | 3.9118 (44) | 39 (15) |
| $L_{\rm bright}$ | $L_\odot$ | 31.6 (14) | 40.7 (14) | 38.5 (16) | 21.06 (72) |
| $L_{\rm dim}$ | $L_\odot$ | 17.46 (78) | 17.99 (62) | 22.63 (95) | 5.1 (10) |
| $(Z/X)_{\rm surf,bright}$ | | 0.0152 (31) | 0.0091 (15) | 0.0173 (32) | 0.00411 (90) |
| $(Z/X)_{\rm surf,dim}$ | | 0.0151 (31) | 0.0091 (15) | 0.0173 (32) | 0.00390 (70) |
| $T_{\rm eff,bright}$ | K | 4848 (42) | 4880 (32) | 4733 (38) | 4982 (35) |
| $T_{\rm eff,dim}$ | K | 4967 (43) | 5041 (33) | 4846 (40) | 5178 (58) |
| $\nu_{\rm max,bright}$ | $\mu$Hz | 62.77 (15) | 52.29 (16) | 48.38 (14) | 76.79 (41) |
| $\nu_{\rm max,dim}$ | $\mu$Hz | 123.22 (32) | 131.31 (46) | 89.63 (27) | 361 (86) |
| Surf. cor. $a_{3,\rm bright}$ | $10^{-6}$ | -0.688 (73) | -0.496 (44) | -0.395 (42) | -0.638 (56) |
| Surf. cor. $a_{-1,\rm bright}$ | $10^{-6}$ | -1.30 (20) | | | |
| Surf. cor. $a_{3,\rm dim}$ | $10^{-6}$ | -0.418 (41) | -0.371 (24) | -0.399 (36) | |
| Surf. cor. $a_{-1,\rm dim}$ | $10^{-6}$ | -0.51 (16) | | | |
| Orbit $i$ [c] | ° | | | | 35.43 (94) |
| Orbit $a$ [c] | $R_\odot$ | | | | 129.6 (42) |

[a] [Fe/H] and [$\alpha$/Fe] from APOGEE DR17 (Abdurro'uf et al. 2022). Adopted metallicity uncertainty is 0.1 dex, since the APOGEE spectra includes companion contamination.
[b] For KIC 2971380, we assumed dY/dZ∼1.5 Brogaard et al. (2012) and $Y_p$ = 0.2470 (Fields et al. 2020), since we did not have independent constraints on the modes of the dim companion.
[c] Including $M_{\rm bright}\sin^3 i$ and $a\sin i$ from Table 1.

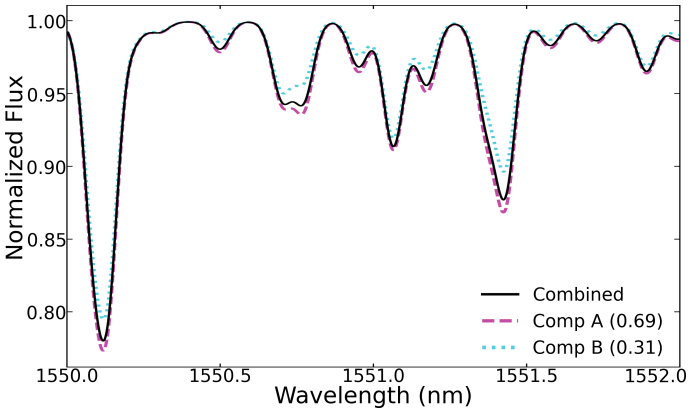


**Fig. 4.** Expected spectroscopic blending of the two stars in KIC 10592924, in the near-infrared.

Kjeldsen & Bedding 1995; Belkacem et al. 2011):

$$\frac{\nu_{\rm max}}{\nu_{\rm max,\odot}} \simeq f_{\nu_{\rm max}} \frac{g}{g_\odot}\left(\frac{T_{\rm eff}}{T_{\rm eff,\odot}}\right)^{-1/2}. \quad (15)$$

We use the solar values $\nu_{\rm max,\odot}$ = 3090$\mu$Hz and $T_{\rm eff}$ = 5772K (Handberg et al. 2017; Prša et al. 2016). The $\nu_{\rm max}$ scaling relation in this form is expected to have systematic uncertainties reflected in the unknown correction factor $f_{\nu_{\rm max}}$ (e.g., Belkacem et al. 2011; Viani et al. 2017), and recent model-dependent asteroseismic inferences of metal-poor stars appear to support this as well (Li et al. 2024; Huber et al. 2024; Larsen et al. 2025). Since we did not include $\nu_{\rm max}$ as an observational constraint for KIC 2971380, we can predict $f_{\nu_{\rm max}}$ using the model-inferred $g$, $T_{\rm eff}$, and observed $\nu_{\rm max}$. This will be a model-dependent estimate, performed under the assumption that the individual-mode-frequency inference represents the ground truth. We used the model-inferred $T_{\rm eff}$ for this test, because we do not have effective temperature observations that were derived while accounting for the companion star. Our stellar model grid uses a fixed solar-calibrated mixing-length value, and a systematic difference between observed and model temperatures would not be unexpected on the RGB. When using this same grid of models, the observed $T_{\rm eff}$ of the red giant in the eclipsing binary KIC 10001167 was ∼ 40K lower than the model-inferred $T_{\rm eff}$ (Thomsen et al. 2025), which is comparable to the statistical uncertainty of our model-inferred $T_{\rm eff}$. When estimating $f_{\nu_{\rm max}}$ this

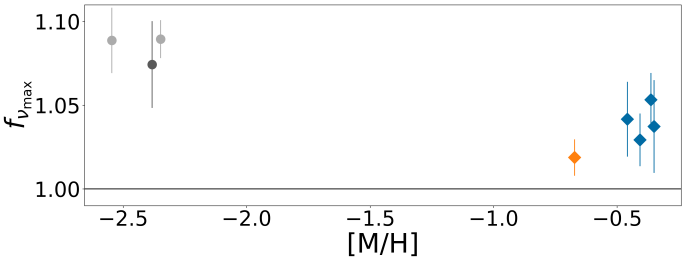


**Fig. 5.** $f_{\nu_{max}}$ estimates for low-metallicity stars (see text for details). Blue: Low metallicity eclipsing binaries (Brogaard et al. 2018, 2022; Thomsen et al. 2022, 2025). Orange: Model inference of KIC 2971380 (this work). Dark grey: Model inference of KIC 8144907 (Huber et al. 2024). Light grey: Model inference of KIC 4671239 & 7693833 (Larsen et al. 2025).

way, we replaced the statistical uncertainty on $T_{\rm eff}$ with 80K in order to simulate the typical accuracy of spectroscopic observations (Bruntt et al. 2010).

With this we derived $f_{\nu_{max}} = 1.019 \pm 0.011$, which is of low significance but indicative of the need for a correction larger than one for metal-poor stars. Particularly if $f_{\nu_{max}}$ is increasing with decreasing metallicity, this would match expectations for the most metal-poor oscillators where much larger corrections have been inferred (Huber et al. 2024; Larsen et al. 2025). We can compare with the most well-studied eclipsing binaries in *Kepler* that also contain a solar-like oscillator, particularly those with the lowest metallicity, KIC 10001167, 4054905, 8430105, and 9970396 (Thomsen et al. 2025; Brogaard et al. 2022; Thomsen et al. 2022; Brogaard et al. 2018). For these eclipsing binaries, the surface gravity measurement is dependent only on the orbital and eclipse modeling, and therefore fully independent of stellar evolutionary models. We show the comparsion in Fig. 5. The eclipsing binaries further support the need for a correction larger than unity for low-metallicity stars.

From the spectroscopy (see Fig. 1), the ratio of the line profile integrals of the binary is roughly 25%. While the exact value is dependent on the assumed spectroscopic template, the true luminosity ratio of the binary is likely within the same order of magnitude. Together with the radial velocity mass ratio, we have used this to estimate the properties of the dimmer companion, assuming $L_{\rm dim}/L_{\rm bright} \sim 0.25 \pm 0.05$ and that the two stellar ages agree to at least 1%. From stellar inference, we estimate that the companion is compatible with a star at the base of the RGB, having $R \sim 2.8 R_\odot$ and $\nu_{\rm max} \sim 361 \pm 86 \mu$Hz. This puts it at or above the Nyquist frequency of *Kepler* long-cadence data. Unfortunately, with an apparent magnitude of $G = 12.6$, the system is far too dim for the TESS photometry to have photometric precision sufficient to measure oscillations from either star. With a future pointing of the PLATO space mission (Rauer et al. 2025), or with the Earth 2.0 telescope (Ge et al. 2022), this system should be considered a strong target of interest for detection of the companion. With the upcoming Gaia Data Release 4, a potential astrometric orbit fit would allow for a fundamental measurement of the mass of the brightest star, providing the first accreted star with solar-like oscillations and an absolute mass measurement. This would make KIC 2971380 an excellent benchmark system for Galactic archaeology and for studying the early merger history, together with the old thick disk eclipsing binary KIC 10001167 (Thomsen et al. 2025).

#### 4.4.2. The asteroseismic binaries, KIC 6501237, 10592924, and 11299484

For KIC 6501237 and 10592924, Fig. D.1 and D.2 in the appendix show the posterior distributions of the dim and bright star. The posterior distribution of KIC 11299484 behaves similarly. In the appendix, Fig. E.1, E.2, E.3, E.4, E.5 and E.6 show the power spectra, observed frequencies, and theoretical frequencies for the three systems. Note that we excluded one radial mode from the brighter star of KIC 6501237, due to its high uncertainty and very low peakbagged amplitude. Given the large uncertainty, it would not have affected the inference results.

When we include only a cubic term to the surface correction, the best fit theoretical frequencies of KIC 6501237 deviate significantly from the observed. For the brighter star, most modes were $1-5\sigma$ different, while for the dimmer component, all modes deviated by 1-1.5$\sigma$. We verified that this discrepancy remains even when fitting the two stars separately. When we include an additional inverse term to the Ball & Gizon (2014) surface correction, we recover a good fit of the modes. However, the inverse term of the brighter star is an order of magnitude larger than the cubic one, which is not expected to be correct (Ball & Gizon 2014). This suggests that the discrepancy stems from a systematic difference between the stellar models and the two stars. Despite this, the seismic inference of KIC 6501237 clearly supports the scenario that the two stars are coeval, as the stellar ages agree far better (0.4%) than expected from the Gaussian prior (5%). If the dimmer set of oscillations are indeed from the dimmer optically resolved star located at $\sim 3$" on-sky separation, the two stars must either be in a very long period orbit, or part of the same stellar association. Based on the predictions of Miglio et al. (2014), all optically resolved asteroseismic binary candidates in *Kepler* should in principle be false positives (chance alignments), and the confirmation of such a system is therefore notable.

For KIC 10592924 and KIC 11299484, we find a statistically reasonable agreement between theoretical and observed oscillation mode frequencies even when using just the cubic correction. The fit quality of the brighter star in KIC 10592924 is only marginally better when including an inverse term. As with KIC 6501237, the inferences clearly confirm that the two stars are coeval.

For all three asteroseismic binaries, it appears to be possible to infer a precise value for the initial helium content (3−4%). We have illustrated this in the corner plots in the appendix (Fig. D.1 and D.2). This was not feasible when studying the two stars in each binary independently. Potentially, the additional constraints offered from the companion oscillator helps resolve degeneracies in the stellar model properties. Since the stars are on the RGB, the treatment of diffusion and gravitational settling is not expected to have a significant impact on the inferred initial helium values, which is generally a major challenge for main sequence seismology (e.g. Verma & Silva Aguirre 2019; Nsamba et al. 2021). In Fig. 6, we compare the inferred helium values to the proto-Sun (Asplund et al. 2009), NGC 6791 (Brogaard et al. 2012), and Big-Bang Nucleosynthesis (Fields et al. 2020). We remark that our choice regarding the surface correction of the brighter star in KIC 10592924 (one-term or two-term) had an impact on the inferred helium value at $\sim 0.9\sigma$ significance. The helium is seen to increase when the inverse surface correction term is included while fitting the brightest star. In addition, the derived helium value of KIC 6501237 is $\sim 2\sigma$ larger than what is expected for the system's metallicity (for illustration, see Fig. 6). Given the need for a large inverse

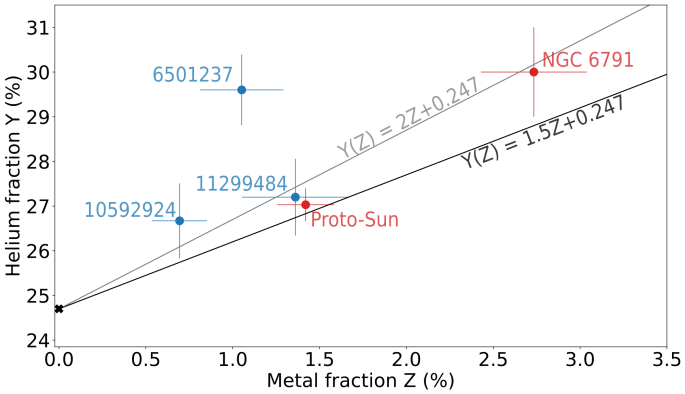


**Fig. 6.** Helium values inferred for the asteroseismic binaries KIC 6501237, 10592924, and 11299484, compared to the proto-Sun (Asplund et al. 2009) and NGC 6791 (Brogaard et al. 2012).

term to the surface effect, we are tempted to conclude that we have over-fitted the seismology of KIC 6501237 with the additional surface term.

For all three stars, the inference of a precise helium value relied on the inclusion of a constraint on $\nu_{\rm max}$ using the asteroseismic scaling relation (eq. (15)). The need for a $\nu_{\rm max}$ constraint might be avoided if we had constraints on the stellar luminosities from photometric and parallactic measurements, however, this is beyond the current scope. Therefore, we will note that these first helium measurements, precise but systematically uncertain, should serve as an encouraging motivation to study asteroseismic binaries. In a future study, we will return to these systems with a detailed modeling effort, in order to account for these effects.

The dimmer companions in both KIC 6501237 and 10592924 show a depression of the dipole mode amplitudes (Fig. E.2, E.4), beyond the general dilution of all the modes due to the contaminating light and granulation signal of the brighter companion. This can be an indication of magnetic activity (e.g., Fuller et al. 2015; Stello et al. 2016). The stellar masses are furthermore compatible with the stars having this effect (Stello et al. 2016).

## 5. Conclusion

Binary stars containing two oscillating RGs offer particularly powerful constraints on models of stellar evolution, if the oscillations of the two stars can be separated in the power spectrum. With high-resolution spectroscopy, we have detected RV variability in 13 candidate binary systems, consistent with them being single-lined or double-lined binaries. Eight of them are also asteroseismic binaries, with three having indications of two overlapping sets of oscillations, four having separate oscillation envelopes, and one (KIC 5015647) showing a very complex power spectrum, but where nearby sources need to be excluded first. Additionally, we confirmed the high-mass evolved oscillator KIC 5978324 (Crawford et al. 2024, 2025) as RV variable based on three spectra obtained over 406 days, with $\mathrm{d}v/\mathrm{d}t = -2.85 \pm 0.05$kms/year. With asteroseismic model inference, we further confirm another two binary systems as coeval, KIC 6501237 and 11299484. We mention two additional binary candidates, KIC 4637699 and 9412408, which have oscillations that are well-separated in frequency, but where we could not conclusively confirm them as RV variable.

With eight spectra of the ex-situ binary KIC 2971380, we were able to constrain the orbital motion, and confirm their mass ratio as consistent with unity. With asteroseismic inference of the bright oscillator, we made predictions for the properties of the dim companion and the orbit, estimating $\nu_{\rm max,dim} \sim 361 \pm 86\mu$Hz, orbit inclination $i \sim 35.4 \pm 0.9°$, and semi-major-axis $130 \pm 4 R_\odot$. We derived an age of $11.7 \pm 1.0$Gyr, consistent with it being $\sim 1.4 \pm 1.1$Gyr older than the thick disk eclipsing binary KIC 10001167 (Thomsen et al. 2025).

We performed a double-seismic inference, utilising the oscillation frequencies of both stars, for three asteroseismic binaries, KIC 6501237, 10592924, and 11299484. This confirmed that the binaries are coeval. From the inference, we obtained precise constraints on their masses ($\sim 1.5\%$), mass ratio ($\sim 1\%$), and the age of the binary ($8-10\%$), while inferring their initial helium content ($\sim 3\%$). For KIC 10592924 and 11299484, we derived helium values consistent with typically assumed linear helium-metallicity relations. Particularly KIC 11299484 agrees very well with proto-Solar predictions (Asplund et al. 2009).

Helium inferred from RGs is not significantly affected by the treatment of diffusion and gravitational settling, which is a major challenge for main sequence seismology (e.g. Verma & Silva Aguirre 2019; Nsamba et al. 2021). The uncertainty in the stellar helium content contributes a large systematic uncertainty to stellar parameters, including the age (see, e.g., Fig. 43 of Lebreton et al. 2014). This impacts several fields relying on accurate stellar model parameters and ages, including Galactic archaeology and exoplanetary studies.

Finally, we remark that both KIC 6501237 and 10592924 show a modulation of the dipole modes of the dim companion. The companion of KIC 10592924, having the highest $\nu_{\rm max}$ of the two systems, presents a suppression of the dipole modes, which is typically an indication of a strong internal magnetic field (Fuller et al. 2015), observed in many red giants and suspected to be due to strong dynamos in the convective core during the main sequence (Stello et al. 2016).

*Acknowledgements.*
We are grateful to Josefina Montalbán for providing a large number of target suggestions for asteroseismic binary candidates to observe, and for helpful comments on the manuscript draft. JST, AMazzi acknowledge support from Bologna University, "MUR FARE Grant Duets CUP J33C21000410001". AMiglio, MMatteuzzi acknowledge support from the ERC Consolidator Grant funding scheme (project ASTEROCHRONOMETRY, `https://www.asterochronometry.eu`, G.A. n. 772293). Based on observations made with the Nordic Optical Telescope, owned in collaboration by the University of Turku and Aarhus University, and operated jointly by Aarhus University, the University of Turku and the University of Oslo, representing Denmark, Finland and Norway, the University of Iceland and Stockholm University at the Observatorio del Roque de los Muchachos, La Palma, Spain, of the Instituto de Astrofisica de Canarias.

## References

Abdurro'uf, Accetta, K., Aerts, C., et al. 2022, ApJS, 259, 35
Appourchaux, T., Antia, H. M., Ball, W., et al. 2015, A&A, 582, A25
Asplund, M., Grevesse, N., Sauval, A. J., & Scott, P. 2009, ARA&A, 47, 481
Ball, W. H. & Gizon, L. 2014, A&A, 568, A123
Beck, P. G., Grossmann, D. H., Steinwender, L., et al. 2024, A&A, 682, A7
Beck, P. G., Kallinger, T., Pavlovski, K., et al. 2018, A&A, 612, A22
Belkacem, K., Goupil, M. J., Dupret, M. A., et al. 2011, A&A, 530, A142
Bell, K. J., Hekker, S., & Kuszlewicz, J. S. 2019, MNRAS, 482, 616
Benbakoura, M., Gaulme, P., McKeever, J., et al. 2021, A&A, 648, A113
Borre, C. C., Aguirre Børsen-Koch, V., Helmi, A., et al. 2022, MNRAS, 514, 2527
Borucki, W. J., Koch, D., Basri, G., et al. 2010, Science, 327, 977
Brogaard, K., Arentoft, T., Jessen-Hansen, J., & Miglio, A. 2021, MNRAS, 507, 496
Brogaard, K., Arentoft, T., Miglio, A., et al. 2023, A&A, 679, A23

Brogaard, K., Arentoft, T., Slumstrup, D., et al. 2022, A&A, 668, A82
Brogaard, K., Hansen, C. J., Miglio, A., et al. 2018, MNRAS, 476, 3729
Brogaard, K., VandenBerg, D. A., Bruntt, H., et al. 2012, A&A, 543, A106
Brown, T. M., Gilliland, R. L., Noyes, R. W., & Ramsey, L. W. 1991, ApJ, 368, 599
Bruntt, H., Bedding, T. R., Quirion, P.-O., et al. 2010, MNRAS, 405, 1907
Choi, J. Y., Espinoza-Rojas, F., Coppée, Q., & Hekker, S. 2025, arXiv e-prints, arXiv:2506.01745
Coelho, P., Barbuy, B., Meléndez, J., Schiavon, R. P., & Castilho, B. V. 2005, A&A, 443, 735
Colman, I. L., Huber, D., Bedding, T. R., et al. 2017, MNRAS, 469, 3802
Corsaro, E. & De Ridder, J. 2014, A&A, 571, A71
Corsaro, E., McKeever, J. M., & Kuszlewicz, J. S. 2020, FAMED: Extraction and mode identification of oscillation frequencies for solar-like pulsators, Astrophysics Source Code Library, record ascl:2006.021
Cox, J. P. & Giuli, R. T. 1968, Principles of stellar structure (New York: Gordon and Breach, 1968)
Crawford, C. L., Bedding, T. R., Li, Y., et al. 2024, MNRAS, 528, 7397
Crawford, C. L., Li, Y., Huber, D., et al. 2025, MNRAS, 542, 3289
Das, P., Hawkins, K., & Jofré, P. 2020, MNRAS, 493, 5195
Dufresne, G., Chaboyer, B., & Rampalli, R. 2026, The Absolute Age of the Open Cluster NGC 6791 and Its Implications for Galactic Archaeology and Asteroseismic Calibration
Espinoza-Rojas, F., Themeßl, N., & Hekker, S. 2025, A&A, 703, A66
Fields, B. D., Olive, K. A., Yeh, T.-H., & Young, C. 2020, J. Cosmology Astropart. Phys., 2020, 010
Foreman-Mackey, D., Hogg, D. W., Lang, D., & Goodman, J. 2013, PASP, 125, 306
Fuller, J., Cantiello, M., Stello, D., Garcia, R. A., & Bildsten, L. 2015, Science, 350, 423
Gaulme, P. & Guzik, J. A. 2019, A&A, 630, A106
Gaulme, P., Jackiewicz, J., Spada, F., et al. 2020, A&A, 639, A63
Gaulme, P., McKeever, J., Jackiewicz, J., et al. 2016, ApJ, 832, 121
Ge, J., Zhang, H., Zang, W., et al. 2022, arXiv e-prints, arXiv:2206.06693
Gehan, C., Godoy-Rivera, D., & Gaulme, P. 2024, A&A, 686, A93
Grossmann, D. H., Beck, P. G., Mathur, S., et al. 2025, A&A, 696, A42
Handberg, R., Brogaard, K., Miglio, A., et al. 2017, MNRAS, 472, 979
Hekker, S., Snellen, I. A. G., Aerts, C., et al. 2008, A&A, 480, 215
Howell, M., Campbell, S. W., Stello, D., & De Silva, G. M. 2024, MNRAS, 527, 7974
Howell, M., Johnson, J. A., Pinsonneault, M. H., et al. 2026, arXiv e-prints, arXiv:2604.27828
Huber, D., Slumstrup, D., Hon, M., et al. 2024, ApJ, 975, 19
Jørgensen, A. C. S., Montalbán, J., Angelou, G. C., et al. 2021, MNRAS, 500, 4277
Kallinger, T., De Ridder, J., Hekker, S., et al. 2014, A&A, 570, A41
Kjeldsen, H. & Bedding, T. R. 1995, A&A, 293, 87
Krishna Swamy, K. S. 1966, ApJ, 145, 174
Larsen, J. R., Rørsted, J. L., Aguirre Børsen-Koch, V., et al. 2025, A&A, 697, A153
Lebreton, Y., Goupil, M. J., & Montalbán, J. 2014, in EAS Publications Series, Vol. 65, EAS Publications Series, ed. Y. Lebreton, D. Valls-Gabaud, & C. Charbonnel (EDP), 99–176
Li, Y., Bedding, T. R., Huber, D., et al. 2024, ApJ, 974, 77
Li, Y., Bedding, T. R., Li, T., et al. 2018, MNRAS, 476, 470
Lund, M. N., Basu, S., Silva Aguirre, V., et al. 2016, MNRAS, 463, 2600
Majewski, S. R., Schiavon, R. P., Frinchaboy, P. M., et al. 2017, AJ, 154, 94
Marcadon, F., Appourchaux, T., & Marques, J. P. 2018, A&A, 617, A2
Mazzi, A., Thomsen, J. S., Miglio, A., et al. 2025, A&A, 699, A39
Miglio, A., Chaplin, W. J., Brogaard, K., et al. 2016, MNRAS, 461, 760
Miglio, A., Chaplin, W. J., Farmer, R., et al. 2014, ApJ, 784, L3
Miglio, A., Chiappini, C., Mackereth, J. T., et al. 2021, A&A, 645, A85
Montalbán, J., Mackereth, J. T., Miglio, A., et al. 2021, Nature Astronomy, 5, 640
Mosser, B., Belkacem, K., Goupil, M. J., et al. 2011, A&A, 525, L9
Mosser, B., Gehan, C., Belkacem, K., et al. 2018, A&A, 618, A109
Mosser, B., Michel, E., Belkacem, K., et al. 2013, A&A, 550, A126
Murphy, S. J., Li, T., Sekaran, S., et al. 2021, MNRAS, 505, 2336
Nielsen, M. B., Davies, G. R., Ball, W. H., et al. 2021, AJ, 161, 62
Nsamba, B., Moedas, N., Campante, T. L., et al. 2021, MNRAS, 500, 54
Paxton, B., Bildsten, L., Dotter, A., et al. 2011, ApJS, 192, 3
Paxton, B. & et al. 2013, ApJS, 208, 4
Paxton, B. & et al. 2015, ApJS, 220, 15
Paxton, B. & et al. 2018, ApJS, 234, 34
Paxton, B. & et al. 2019, ApJS, 243, 10
Pires, S., Mathur, S., García, R. A., et al. 2015, A&A, 574, A18
Prša, A., Harmanec, P., Torres, G., et al. 2016, AJ, 152, 41
Rauer, H., Aerts, C., Cabrera, J., et al. 2025, Experimental Astronomy, 59, 26
Rendle, B. M., Buldgen, G., Miglio, A., et al. 2019, MNRAS, 484, 771
Rucinski, S. 1999, in Astronomical Society of the Pacific Conference Series, Vol. 185, IAU Colloq. 170: Precise Stellar Radial Velocities, ed. J. B. Hearnshaw & C. D. Scarfe, 82
Salaris, M., Chieffi, A., & Straniero, O. 1993, ApJ, 414, 580
Schimak, L. S., Bedding, T. R., Crawford, C. L., et al. 2026, MNRAS, 546, stag151
Schonhut-Stasik, J., Huber, D., Baranec, C., et al. 2020, ApJ, 888, 34
Scuflaire, R., Théado, S., Montalbán, J., et al. 2008, Ap&SS, 316, 83
Stello, D., Bedding, T. R., & Gilliland, R. L. 2026, MNRAS[arXiv:2603.13701]
Stello, D., Cantiello, M., Fuller, J., et al. 2016, Nature, 529, 364
Tailo, M., Corsaro, E., Miglio, A., et al. 2022, A&A, 662, L7
Tayar, J., Ceillier, T., García-Hernández, D. A., et al. 2015, ApJ, 807, 82
Telting, J. H., Avila, G., Buchhave, L., et al. 2014, Astronomische Nachrichten, 335, 41
Themessl, N., Hekker, S., Mints, A., et al. 2018, ApJ, 868, 103
Themeßl, N., Hekker, S., Southworth, J., et al. 2018, MNRAS, 478, 4669
Thomsen, J. S., Brogaard, K., Arentoft, T., et al. 2022, MNRAS, 517, 4187
Thomsen, J. S., Miglio, A., Brogaard, K., et al. 2025, A&A, 699, A152
Townsend, R. H. D. & Teitler, S. A. 2013, MNRAS, 435, 3406
Verma, K. & Silva Aguirre, V. 2019, MNRAS, 489, 1850
Viani, L. S., Basu, S., Chaplin, W. J., Davies, G. R., & Elsworth, Y. 2017, ApJ, 843, 11
White, T. R., Benomar, O., Silva Aguirre, V., et al. 2017, A&A, 601, A82
Willett, E., Miglio, A., Khan, S., et al. 2026, MNRAS[arXiv:2602.06870]

**Table A.1.** Systems monitored with FIES over multiple nights. Double-lined (called SB2) model fits were only attempted on visually bimodal spectra. If an SB2 model was used, the single-lined (SB1) results are not reported (except for $\Delta\sigma$). Velocity units are in km/s unless specified.

| KIC | $\frac{\Delta\sigma}{\mathrm{Err}}$ [a,b] | $v$ [c] | $\Delta v$ [b,c] | $\frac{dv}{dt}$ (kms/yr) [c,d] | $\Delta$BIC [e] | baseline (days) | # [f] | model |
|---|---|---|---|---|---|---|---|---|
| Significant variability | | | | | | | | |
| 2971380 | 17.7 | 35.01 | 43.26 (22) | 49.41 (63) | -6238 | 189 | 7 | SB2 |
| 4260884 | 20.8 | 3.16 | 3.16 (27) | 6.83 (63) | -116 | 180 | 4 | SB2 |
| 5300269 | 4.4 | 2.89 | 4.1 (10) | -7.8 (18) | -18 | 201 | 3 | SB2 |
| 7697607 | 4.5 | 9.78 | 0.338 (90) | -0.367 (72) | -24 | 343 | 3 | SB2 |
| 8479182 | 1.1 | 11.92 | 0.377 (98) | -0.333 (92) | -12 | 351 | 5 | SB2 |
| 8479383 | 50 | 11.82 | 8.19 (14) | 10.78 (18) | -3551 | 275 | 4 | SB2 |
| 8649099 | 12.0 | 9.82 | 0.730 (78) | 0.923 (99) | -86 | 286 | 5 | SB2 |
| 10592924 | 0.90 | 4.8 | 9.4 (10) | 25.1 (27) | -89 | 137 | 2 | SB2 |
| 4346953 | 0.2 | -0.8 | 2.772 (75) | -7.08 (19) | -1369 | 143 | 2 | SB1 |
| 4659808 | 3.8 | 19.5 | 2.233 (80) | -5.59 (20) | -771 | 146 | 2 | SB1 |
| 5015647 | 1.9 | -32.0 | 7.230 (75) | -18.75 (20) | -9272 | 141 | 2 | SB1 |
| 5978324 | 2.5 | 18.7 | 3.199 (75) | -2.845 (58) | -2376 | 406 | 3 | SB1 |
| 8181509 | 0.1 | -31.2 | 0.268 (72) | 0.237 (64) | -13 | 413 | 2 | SB1 |
| Tentative indication of variability | | | | | | | | |
| 11299484 | 2.3 | 5.66 | 0.45 (22) | 0.35 (17) | -2.8 | 255 | 3 | SB2 |
| 4637699 | 1.0 | -97.0 | 0.28 (19) | 0.55 (41) | -0.4 | 146 | 2 | SB1 |
| 6501237 [g] | 9.5 | -7.3 | 0.228 (81) | -0.49 (18) | -7.2 | 170 | 2 | SB1 |
| 9392647 [h] | 1.6 | -44.7 | 0.27 (13) | 2.1 (10) | -2.7 | 42 | 2 | SB1 |
| 9392650 [h] | 0.7 | -83.5 | 0.39 (14) | 3.4 (12) | -7.4 | 42 | 2 | SB1 |
| 9412408 | 1.1 | 10.3 | 0.125 (75) | -0.18 (11) | -2.0 | 259 | 2 | SB1 |
| 11352644 | 3.3 | -52.0 | 0.047 (86) | -0.033 (88) | 1.2 | 300 | 2 | SB1 |
| Insignificant variability | | | | | | | | |
| 6369592 | 3.7 | 21.12 | 0.65 (20) | -0.11 (14) | 1.4 | 413 | 4 | SB2 |
| 2442606 | 1.3 | 16.5 | 0.035 (75) | 0.22 (47) | 0.5 | 58 | 2 | SB1 |
| 4157282 | 2.9 | -19.6 | 0.011 (86) | -0.03 (26) | 0.7 | 119 | 2 | SB1 |
| 4159205 | 1.5 | -62.8 | 0.019 (73) | 0.013 (89) | 1.4 | 259 | 2 | SB1 |
| 5024272 | 1.2 | 4.5 | 0.058 (76) | -0.23 (29) | 0.1 | 94 | 2 | SB1 |
| 5202286 | 2.0 | 16.6 | 0.078 (88) | -0.09 (11) | -0.1 | 307 | 2 | SB1 |
| 5353108 | 1.9 | -50.5 | 0.051 (72) | -0.15 (21) | 0.2 | 126 | 2 | SB1 |
| 5630997 | 0.2 | 9.3 | 0.03 (14) | 0.05 (22) | 0.6 | 227 | 2 | SB1 |
| 6206407 | 1.8 | -47.7 | 0.024 (75) | 0.04 (12) | 0.6 | 227 | 2 | SB1 |
| 6208846 | 1.7 | -7.8 | 0.045 (73) | 0.12 (19) | 0.3 | 143 | 2 | SB1 |
| 6221548 | 0.7 | -41.2 | 0.040 (75) | 0.11 (21) | 0.4 | 133 | 2 | SB1 |
| 6526377 | 1.1 | -6.0 | 0.011 (74) | 0.02 (10) | 0.7 | 262 | 2 | SB1 |
| 8708536 | 0.8 | -18.0 | 0.029 (72) | -0.04 (10) | 0.5 | 263 | 2 | SB1 |
| 9205419 | 2.5 | -4.7 | 0.070 (76) | 0.038 (67) | 1.3 | 276 | 3 | SB1 |
| 9775927 | 1.1 | -10.0 | 0.005 (72) | 0.01 (10) | 0.7 | 259 | 2 | SB1 |
| 10464837 | 1.7 | -22.4 | 0.050 (76) | 0.048 (76) | 0.99 | 297 | 2 | SB1 |
| 11136690 | 2.3 | -59.3 | 0.044 (76) | 0.014 (97) | 1.4 | 255 | 3 | SB1 |

[a] Difference in width of a Gaussian model fit, scaled by uncertainty, assuming only one spectral line.
[b] Most significant difference between two spectra.
[c] For SB1 models, this is measured in RV. For SB2 models, this is based on $\Delta v = RV_2 - RV_1$.
[d] Slope of a linear fit.
[e] Difference between Bayesian information criterion of a linear and a constant fit. Negative favors the linear.
[f] Number of observed nights.
[g] KIC 6501237 has a nearby star with similar RV, and seeing conditions were significantly different for the two nights.
[h] KIC 9392647 and 9392650 are very close on the sky, and was likely selected as candidate asteroseismic binaries because of that. While their RVs are different, their proximity might have affected the observation quality.

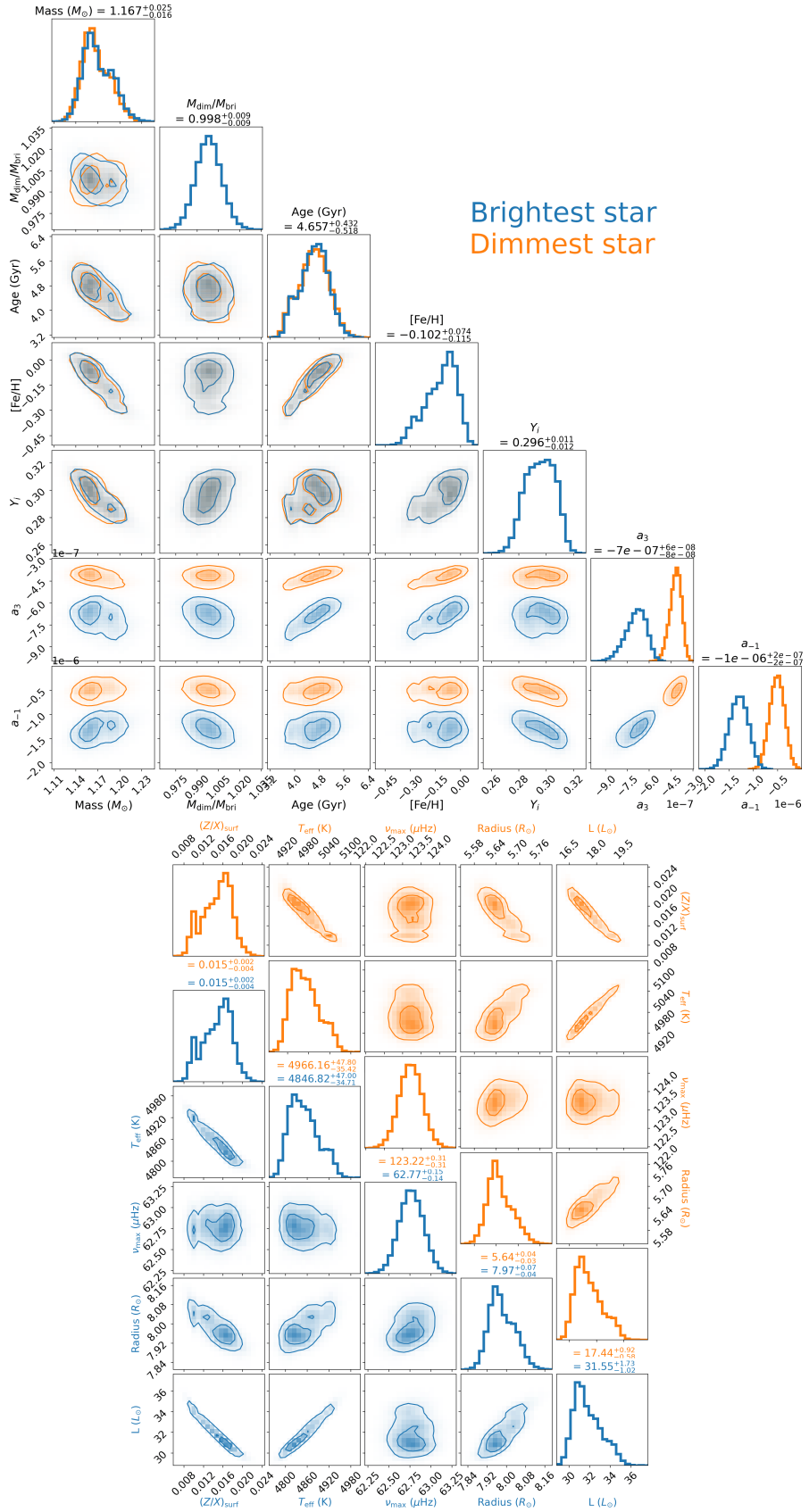


**Fig. D.1.** Corner plot of the asteroseismic inference of both stars in KIC 6501237. Top: Comparison on the fit parameters, mass, age, metallicity, helium, and surface corrections. Middle: Derived parameters for the dimmest star. Bottom: Derived parameters for the brightest star.

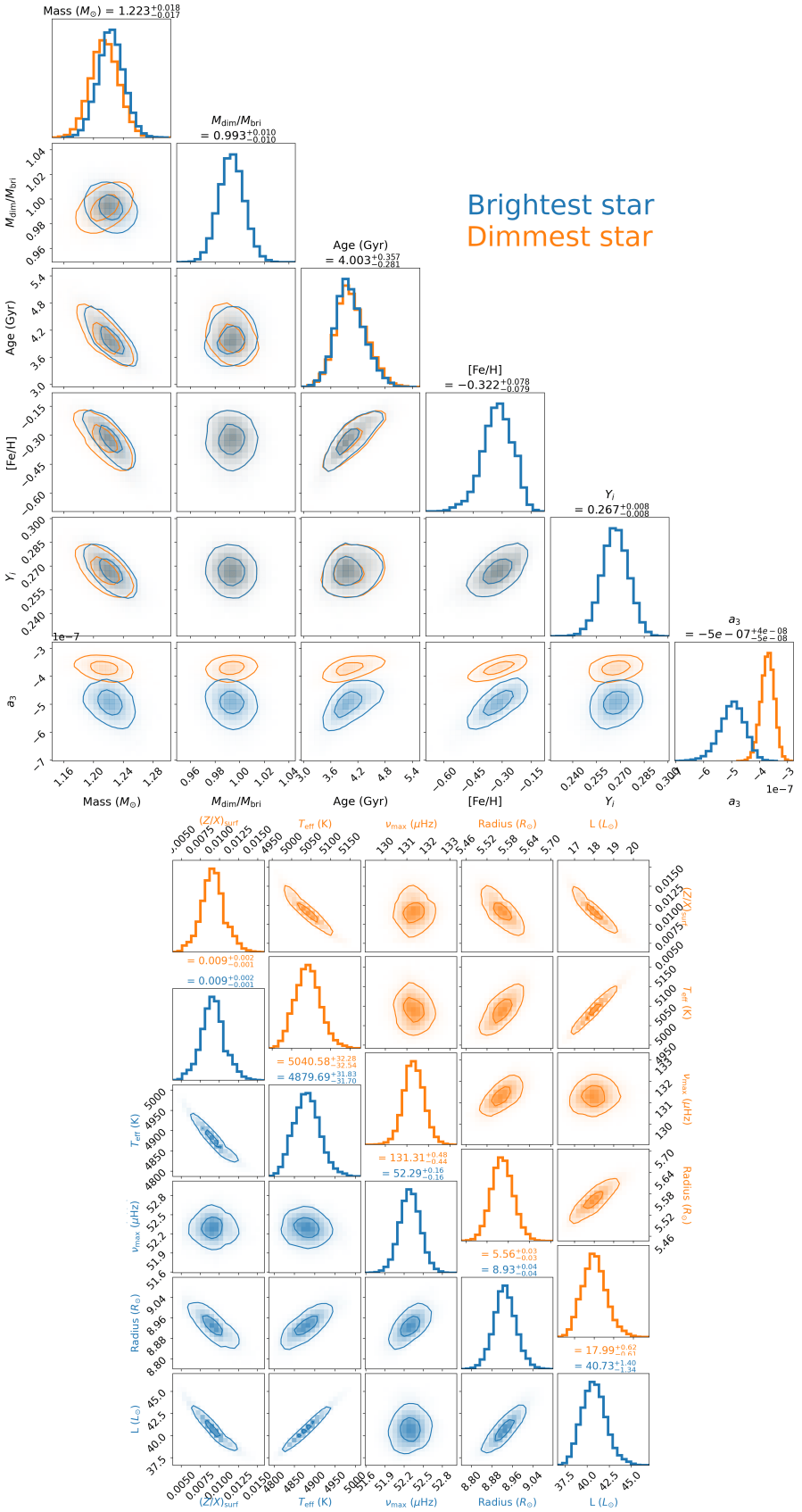


**Fig. D.2.** Corner plot of the asteroseismic inference of both stars in KIC 10592924. Top: Comparison on the fit parameters, mass, age, metallicity, helium, and surface corrections. Middle: Derived parameters for the dimmest star. Bottom: Derived parameters for the brightest star.

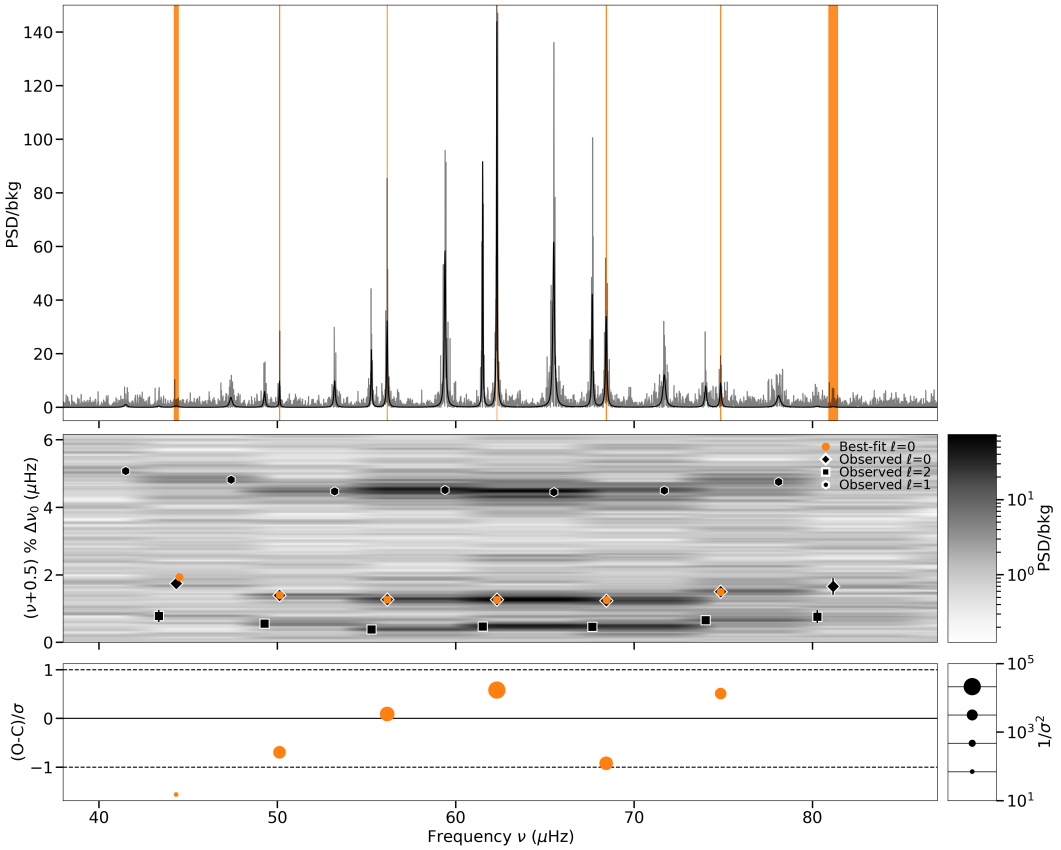


**Fig. E.1.** Same as Fig. 3, but for the brightest star of KIC 6501237.

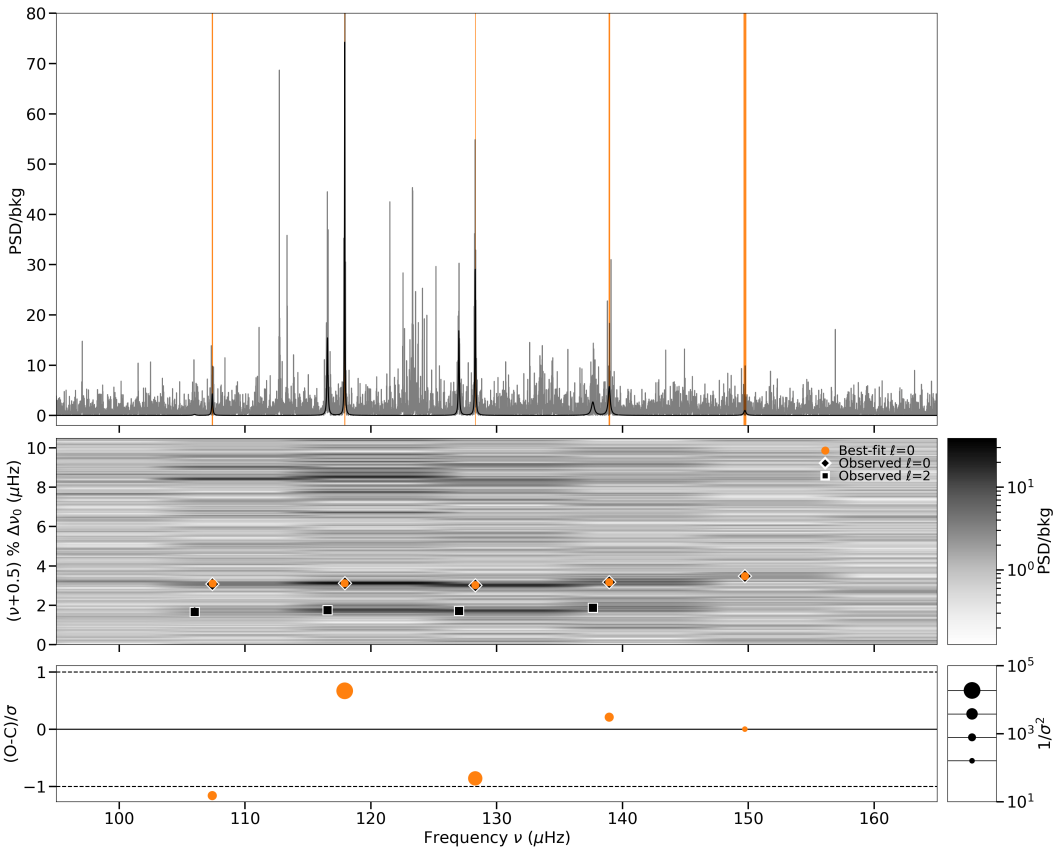


**Fig. E.2.** Same as Fig. 3, but for the dimmest star of KIC 6501237.

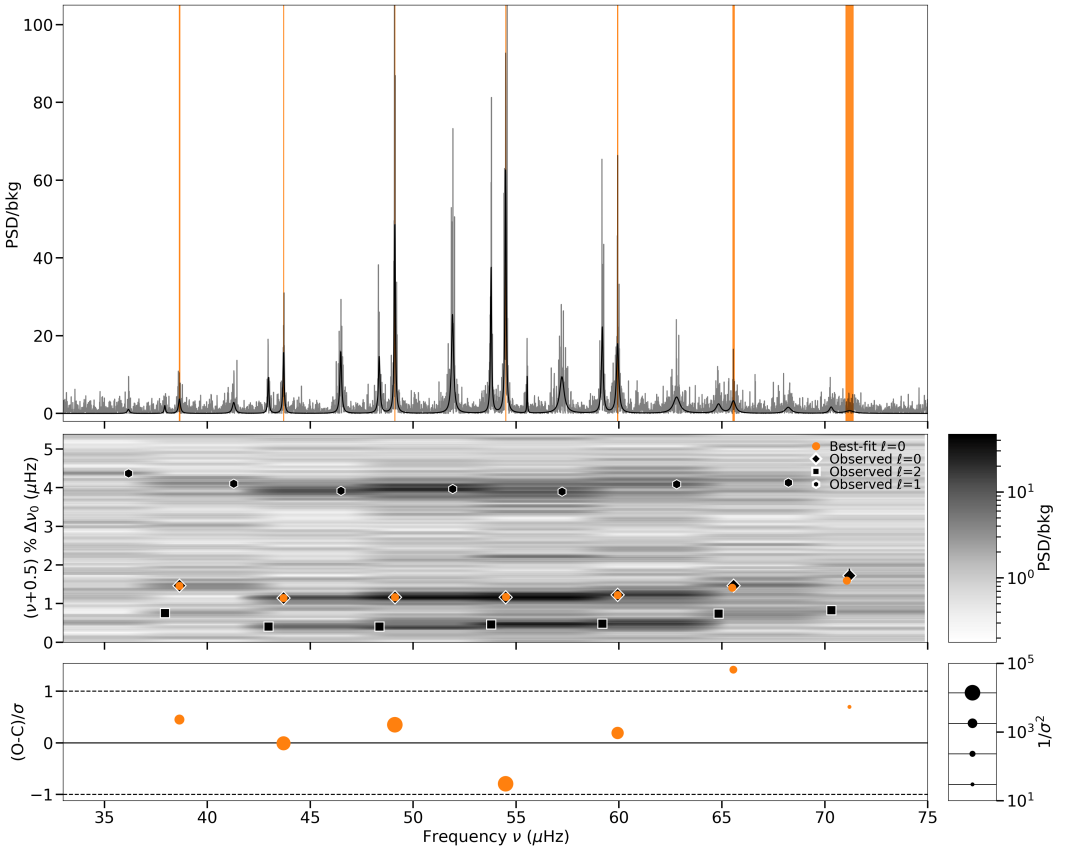


**Fig. E.3.** Same as Fig. 3, but for the brightest star of KIC 10592924.

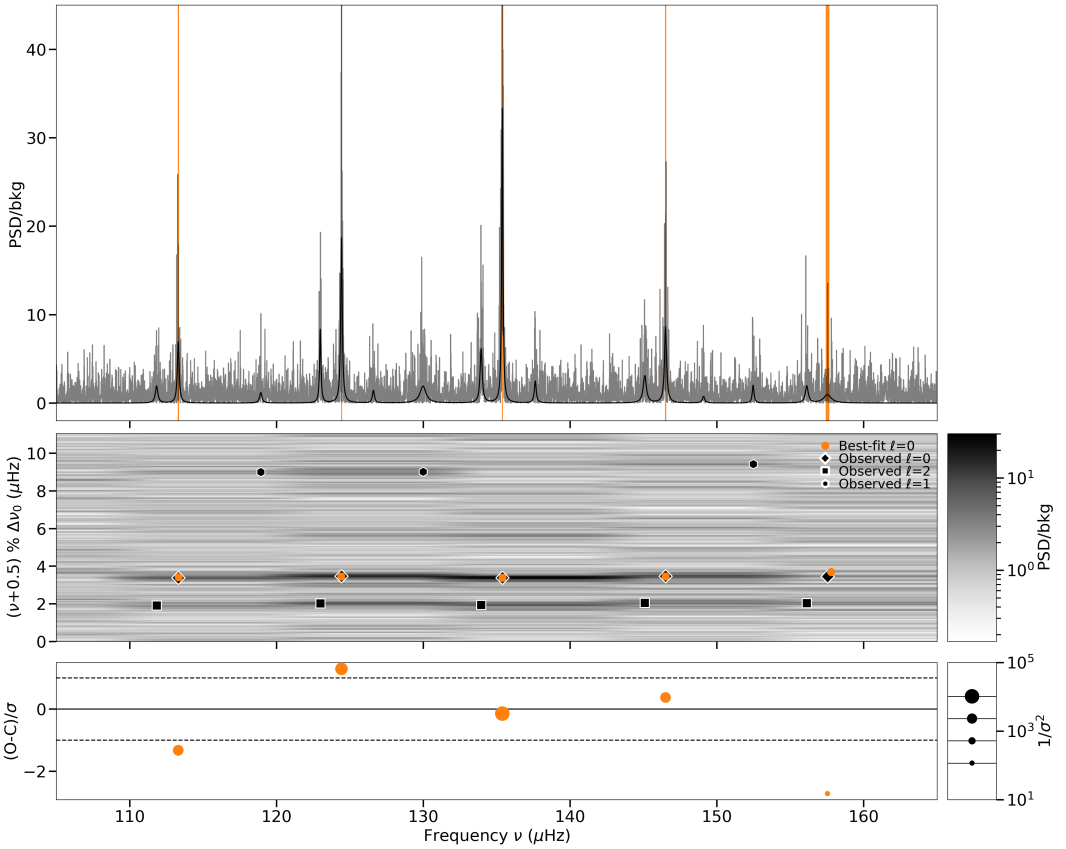


**Fig. E.4.** Same as Fig. 3, but for the dimmest star of KIC 10592924.

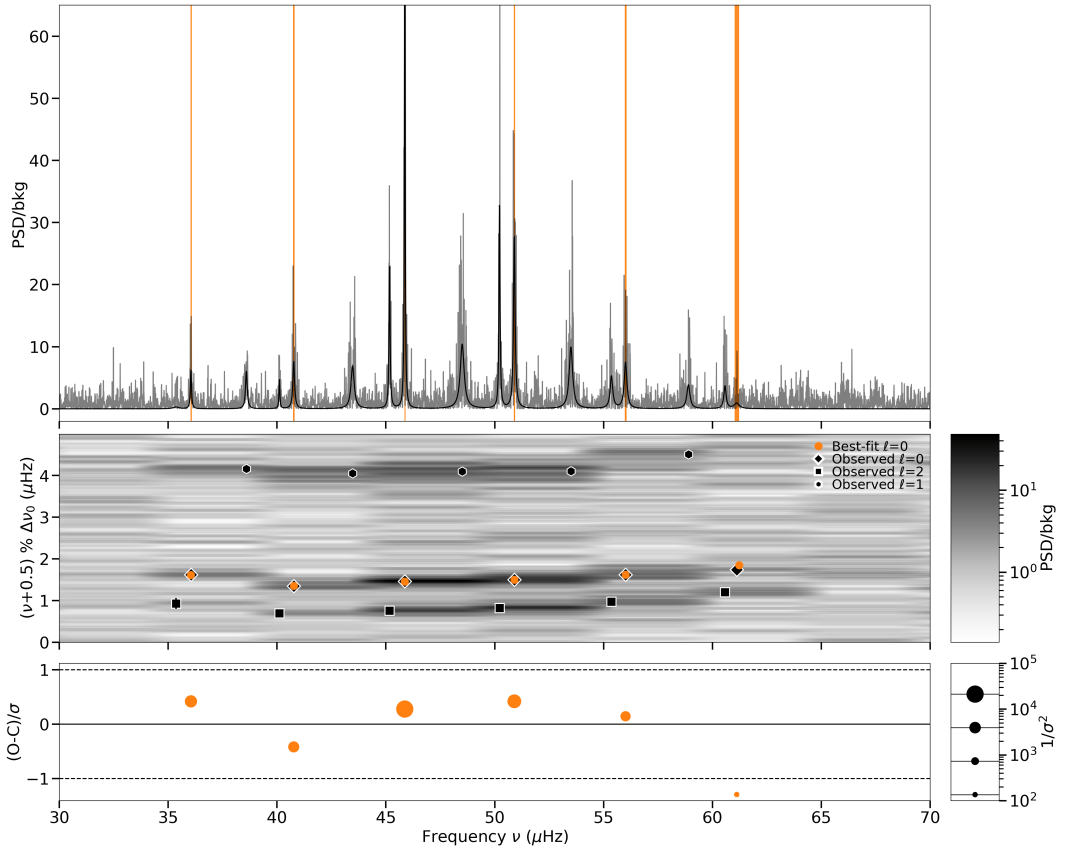


**Fig. E.5.** Same as Fig. 3, but for the brightest star of KIC 11299484.

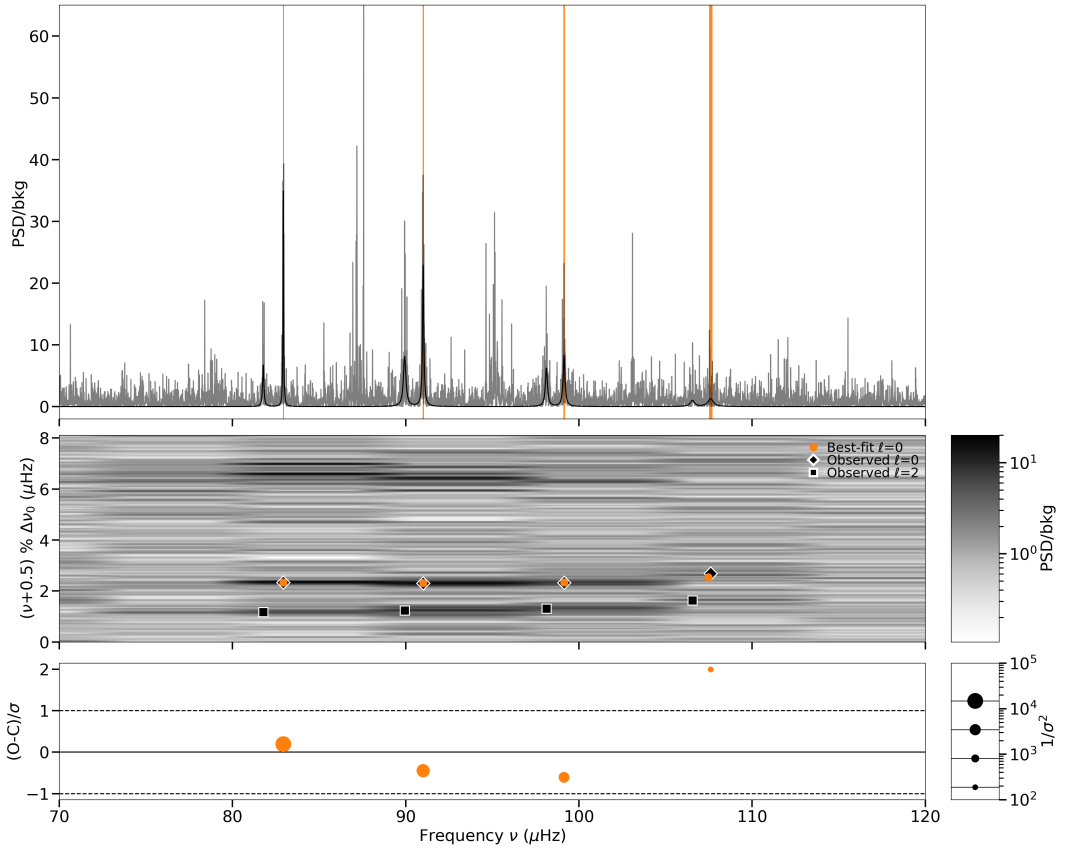


**Fig. E.6.** Same as Fig. 3, but for the dimmest star of KIC 11299484.

**Table B.1.** Radial velocities for KIC 2971380. X=2460000 days. RV units are in km/s.

| BJD-X | RV (bright) | RV (dim) | Cov ($km^2/s^2$) |
|---|---|---|---|
| 744.7479 | -3.778 (79) | 15.38 (33) | 0.00595 |
| 798.7172 | 16.169 (87) | -4.30 (34) | -0.00570 |
| 839.6515 | 13.420 (75) | -1.35 (27) | 0.00674 |
| 848.5864 | 10.030 (66) | 1.70 (28) | 0.00888 |
| 862.7040 | 3.20 (10) | 9.25 (45) | 0.00709 |
| 863.4471 | 2.711 (64) | 9.56 (27) | 0.00458 |
| 888.5140 | -11.547 (52) | 23.37 (20) | -0.00002 |
| 933.5083 | 17.77 (20) | -6.03 (77) | 0.00675 |

**Table C.1.** Peakbagged frequencies for binaries.

| $\ell$ | KIC 6501237 | KIC 10592924 | KIC 2971380[a] |
|---|---|---|---|
| 1 | 41.497 (52) | 36.168 (27) | |
| 2 | 43.36 (18) | 37.937 (26) | |
| 0 | 44.33 (12) | 38.646 (22) | 57.031 (19) |
| 1 | 47.398 (27) | 41.284 (29) | |
| 2 | 49.284 (17) | 42.967 (12) | 63.372 (48) |
| 0 | 50.123 (13) | 43.704 (10) | 64.497 (16) |
| 1 | 53.209 (15) | 46.484 (13) | |
| 2 | 55.2724 (92) | 48.353 (13) | 71.2577 (81) |
| 0 | 56.1564 (97) | 49.1114 (84) | 72.4132 (70) |
| 3? | | | 73.732 (19) |
| 1 | 59.398 (10) | 51.915 (12) | |
| 2 | 61.5104 (69) | 53.7870 (87) | 79.143 (11) |
| 0 | 62.3054 (69) | 54.4933 (85) | 80.2257 (90) |
| 3? | | 55.5410 (74) | |
| 1 | 65.491 (11) | 57.229 (23) | |
| 2 | 67.6551 (96) | 59.189 (12) | 87.183 (30) |
| 0 | 68.432 (11) | 59.935 (14) | 88.227 (16) |
| 3? | | | 89.605 (85) |
| 1 | 71.688 (19) | 62.799 (33) | |
| 2 | 74.007 (19) | 64.836 (53) | 95.19 (11) |
| 0 | 74.851 (16) | 65.559 (37) | 96.355 (30) |
| 1 | 78.102 (33) | 68.223 (69) | |
| 2 | 80.26 (19) | 70.310 (64) | |
| 0 | 81.16 (25) | 71.20 (18) | |
| 2 | 105.99 (22) | 111.832 (42) | |
| 0 | 107.396 (26) | 113.306 (18) | |
| 1 | | 118.929 (51) | |
| 2 | 116.552 (14) | 122.984 (15) | |
| 0 | 117.9211 (73) | 124.429 (13) | |
| 3? | | 126.603 (42) | |
| 1 | | 129.980 (51) | |
| 2 | 126.996 (12) | 133.943 (21) | |
| 0 | 128.297 (10) | 135.3836 (98) | |
| 3? | | 137.630 (28) | |
| 2 | 137.645 (46) | 145.090 (32) | |
| 0 | 138.945 (26) | 146.506 (19) | |
| 3? | | 149.094 (75) | |
| 1 | | 152.470 (33) | |
| 2 | | 156.126 (42) | |
| 0 | 149.727 (79) | 157.533 (92) | |

[a] $\ell$=1 frequencies are reported in Table C.2.

**Table C.2.** Peakbagged $\ell$=1 frequencies for KIC 2971380.

| | | | |
|---|---|---|---|
| 67.370 (19) | 75.0051 (61) | 81.5798 (71) | 91.686 (23) |
| 68.071 (14) | 75.3706 (60) | 82.034 (64) | 92.191 (29) |
| 68.3396 (68) | 75.7982 (45) | 82.495 (63) | 92.615 (19) |
| 68.8495 (59) | 76.1408 (54) | 82.959 (16) | 93.0945 (73) |
| 69.1612 (18) | 76.4875 (48) | 83.4818 (43) | |
| 69.4833 (56) | 76.8045 (63) | 83.9627 (89) | |
| 69.8227 (96) | 77.1701 (28) | 84.3387 (64) | |
| | 77.5727 (79) | 84.6943 (53) | |
| | 77.9867 (48) | 85.1309 (69) | |
| | | 85.552 (21) | |